ICARUS 108, 59–80 (1994)

Is There a Planet around β Pictoris? Perturbations of a Planet on a Circumstellar Dust Disk

2. The Analytical Model

DANIELA LAZZARO

Observatório Nacional, DAF, 20921 Rio de Janeiro, Brazil, and Observatoire de Paris, DAEC/EUROPA, 92195 Meudon Cedex, France

BRUNO SICARDY

Observatoire de Paris, DAEC/EUROPA, 92195 Meudon Cédex, France, and Université Pierre et Marie Curie, 75005 Paris Cédex, France

FRANÇOISE ROQUES

Observatoire de Paris, DAEC/EUROPA, 92195 Meudon Cédex, France
E-mail: roques@mesioa.obspm.circe.fr

AND

RICHARD GREENBERG

University of Arizona, Lunar and Planetary Laboratory, Tucson, Arizona 85721

Received July 6, 1993; revised January 7, 1994

The evolution of micrometer-sized circumstellar grains orbiting β Pictoris is studied, taking into account the combined effects of first order resonances due to a hypothetical planet and the dissipative effect due to Poynting–Robertson drag. We first derive the averaged equations of motion of the grain near a resonance, and we describe qualitatively and quantitatively the capture into the resonance (mechanism of entrance, time scales for capture, etc.).

It appears that the probability of capture cannot be derived analytically, because of the nonadiabaticity of the motion at the entrance into the resonance, at least for micrometer-sized particles and planet masses smaller than about one saturnian mass.

We show that the capture of a grain into a resonance critically depends (i) on the orbital eccentricity and (ii) on the value of the critical argument of resonance just at the entrance into the resonance. Maps of capture/noncapture regions vs these two parameters are derived numerically for the 1:2, 2:3, and 3:4 resonances. They show the complexity of the capture regions, and indicate that uranian or larger planets are able to trap most of the grains into the 1:2 resonance, while ~5 Earth masses are sufficient to trap grains into the 3:4 resonance for any grain with initial eccentricities smaller than a few percent. These results underline the dynamical importance of small planetary objects embedded in circumstellar dust disks.

1. INTRODUCTION

Dissipative effects, when combined with resonance phenomena, may lead to complex dynamics, whose importance for the evolution of small bodies of the Solar System was recognized long ago. Among this class of phenomena, one can note the tidal evolution of satellites (see the review by Peale 1986) and the energy and angular momentum exchange between a collisional ring and a satellite (see the reviews by Goldreich and Tremaine 1982, Borderies *et al.* 1984, and Meyer-Vernet and Sicardy 1987). Another mechanism, more relevant to the early Solar System dynamics, is the trapping and eccentricity pumping of planetesimals, under the simultaneous influence of gas drag and resonances with a jovian planet (Greenberg 1978, Weidenschilling and Davis 1985, Patterson 1987, Beaugé and Ferraz-Mello 1993, and Kary *et al.* 1993, and see the review by Malhotra 1993).

In the same class of problems, one can think of the decay of small particles (a few to several micrometers in size) due to radiation forces, and more specifically to Poynting–Robertson (PR) drag. This decay may be followed by a capture into a resonance with a planet. The

0019-1035/94 $6.00

latter problem, although it bears some formal resemblance to the gas drag problem, has some specifications of its own that we would like to study in this paper.

One of the main differences between PR drag and gas drag is that the latter is proportional to the *relative* velocity (or its square, depending on the regime) of the body with respect to the gas, while the PR drag is proportional to the *absolute* velocity of the particle in an intertial frame (see Eq. (5)). Since the gas is roughly moving at a Keplerian rate, the gas drag will tend to rapidly damp the particle's orbital eccentricity, while keeping the semimajor axis roughly constant during this damping. In contrast the PR drag damps at about the same rate the eccentricity and the semimajor axis (Burns *et al.* 1979). A second difference involves the time scale for each damping. In the case of gas drag, significant orbital damping for meter-sized particles in the primordial solar nebula can occur in times as short as ~100 years (Weidenschilling 1977). In the case of PR drag, the lifetime of micrometer-sized particles at the level of the giant planets may be as large as a million years (see Eq. (32)). As a consequence, eccentricities can be pumped up to large values in the case of PR drag with resonant forcing, leading to the deep crossing of the planet orbit, and ejection from the resonance through close encounter with the planet (Sicardy *et al.* 1993, Weidenschilling and Jackson 1993). In contrast, gas drag can lead to equilibrium orbits with moderate eccentricities, near a mean motion resonance (Weidenschilling and Davis 1985, Patterson 1987). Finally, the usual expansions in (small) eccentricity used for studying resonant effects near circular motion with gas drag are no longer valid for PR drag. Thus numerical integration becomes necessary.

Another important point is the universality of radiation forces. In view of the robustness of their intensity against variation in the particle properties, this study can be applied to a wide variety of problems. One of them is the continuous influx of asteroidal and cometary grains into resonance regions with planets through Poynting–Robertson drag. Pioneering work in this field has been performed by Gonczi *et al.* (1982), Jackson and Zook (1989), and more recently, by Jackson and Zook (1992) and Dermott *et al.* (1992). Interestingly enough, IRAS observations now indicate that asteroidal dust may be trapped in resonances with the Earth (see Dermott *et al.* 1993a, 1993b).

Another situation of interest is the presence of grains in circumstellar disks. More observational data are likely to be available quite soon on these objects. It is thus important to better understand the dynamics of these disks, since they can represent various stages of protoplanetary systems. Of course, the full problem, including accretion, collisions, mutual gravitational of planetesimals, gas drag, etc., is very complex.

In this paper, we focus instead on one particular problem, namely the decay of circumstellar grains due to Poynting–Robertson drag and their possible capture into mean motion resonances with a hypothetical planet orbiting the star. For this approach to be valid, we assume that the gas from the protosolar nebula has been cleared, so that the associated drag can be discarded. Also, we have to assume that the optical thickness of the disk is small enough so that mutual collisions do not play an important role. A previous paper by Scholl *et al.* 1993, and a companion paper by Roques *et al.* 1994 (hereafter referred to as Paper I) presents numerical results on the orbital evolution of noninteracting grains around the star β Pictoris. The parallel architecture of the computer (a Connection Machine) makes it possible to integrate the exact equations of motion of more than 8,000 particles at a time, thus making visible collective patterns driven by the alleged planet.

To understand these structures more easily, we have to simplify the problem as much as possible in this paper, keeping, however, the relevant physics at work. To do so, we study the system formed by the central star, a planet orbiting it, and a dust grain of negligible mass, moving in the planetary orbital plane (planar problem). We neglect the interactions between the grains themselves, in particular the collisions. Even so, the problem is rich enough to deserve some careful attention. The questions that we would like to answer are then the following:

- What is the *minimum* planetary mass necessary to trap (even temporarily) a grain into a resonance?
- Are there *equilibrium* orbits in which a grain could be trapped permanently?
- Even if the trapping is not permanent, it is *long enough* to explain a statistical accumulation of dust material at the resonances?
- For some initial distribution of orbital elements, what is the *probability* of capture of a grain into a resonance?

Our approach is semianalytical in the sense that we first derive the averaged equations of motion, keeping only the resonant terms in the perturbing function. We then integrate the resulting set of differential equations numerically. The advantages of such an approach are twofold. First, it is much faster, from a computational point of view, than the integration of the exact equations of motion, since short period terms have been averaged out. Second, from a more physical point of view, the averaged equations keep only the dynamically relevant terms of the perturbing function, allowing one to better disentangle local, unimportant behavior from global trends which will have statistical effects on the disk structure.

The price to pay is that the perturbing function has to be truncated at some order in eccentricity, which invalidates its use at high eccentricity. Thus our aim here is restricted to better understanding the *entrance* into the resonances, when the orbital eccentricity of the grain is still small. Numerical simulations such as those presented

in Paper I can then give some support to analytical results, or on the other hand suggest new directions of research.

In the next section, we derive analytically the averaged equations of motion. Section 3 is devoted to a more qualitative and physical understanding of the resonance vs dissipation dynamics. Numerical integrations, using the parameters of grains around the star β Pictoris, are described in Section 4. The mechanism of entrance into the resonance, together with the probability of capture, is investigated in Section 5. A brief discussion and some conclusions are given in Section 6. An appendix gives a list of the symbols used in this paper, as well as in Paper 1.

2. ANALYTICAL APPROACH

2.1. *The Poynting–Robertson Drag*

The radiation force, due to the stellar photons hitting a grain, is given by (see, e.g., the extensive discussion by Burns *et al.* 1979)

$$\mathbf{F}_{\rm rad} = \left(\frac{S\sigma}{c}\right) Q \left[\left(1 - \frac{\dot{r}}{c}\right)\mathbf{u}_{\rm r} - \frac{\mathbf{v}}{c}\right], \tag{1}$$

where S is the energy flux at the grain, σ is its cross section, c is the speed of light, Q is the radiation pressure efficiency, $\dot{r}$ and $\mathbf{v}$ are the radial and total velocity of the grain, respectively, $\mathbf{u}_{\rm r}$ is the unit vector in the direction of the incident radiation, and r is the distance to the star. In the above expression, the constant radial term is usually referred to as the radiation pressure, while the velocity-dependent part is the Poynting–Robertson (PR) drag. Because S varies as $1/r^2$, one can define the coefficient β as the constant ratio between the radiation pressure and the gravitational force,

$$\beta \equiv \frac{S\sigma Q}{c} \Big/ \frac{\mathcal{G}M_\star m_{\rm g}}{r^2}, \tag{2}$$

where $\mathcal{G}$ is the gravitational constant and $m_{\rm g}$ and $M_\star$ are the masses of the grain and the star, respectively. The origin of the reference frame is considered to be at the star's center. The radiation force is therefore given by

$$\mathbf{F}_{\rm rad} = \left(\frac{\mathcal{G}M_\star m_{\rm g}\beta}{r^2}\right)\left[\left(1 - \frac{\dot{r}}{c}\right)\mathbf{u}_{\rm r} - \frac{\mathbf{v}}{c}\right]. \tag{3}$$

The net effect of the radiation pressure is to modify, by a factor of $1 - \beta$, the mass of the central body as perceived by the grain. Thus, the larger the coefficient β, the smaller the apparent mass of the central body felt by the grain.

Three approximations are made to derive the equations of motion given in the next Section. A first approximation is to consider that the dissipation coefficient

$$\alpha \equiv \frac{\mathcal{G}M_\star\beta}{r^2 c} \tag{4}$$

is constant along the orbit, and is calculated by replacing r by the semimajor axis $a_{\rm g}$ of the grain orbit. This is valid as long the orbital eccentricity of the grain remains small.

A second approximation is then to consider the PR drag force as given by

$$\mathbf{F}_{\rm PR} = -m_{\rm g}\alpha\mathbf{v}, \tag{5}$$

i.e., to drop the term $-(\dot{r}/c)\mathbf{u}_{\rm r}$ in Eq. (3). This is a reasonable assumption if we admit again a small orbital eccentricity for the grain, since $-(\dot{r}/c)\mathbf{u}_{\rm r}$ averages to zero during one orbital period, at first order in eccentricity.

Finally, one can note that Eq. (3) neglects the stellar wind drag, which would require a multiplicative factor $1 + {\rm sw}$ in front of the term $-\mathbf{v}/c$ in the above equation, where sw is the ratio of stellar wind drag to PR drag (Jackson and Zook 1992). This ratio is 0.3 in the case of the solar wind drag. In the general case, however, or even in the more specific case of β Pictoris studied here, we have no information on this ratio. Its value may actually be absorbed into the dissipation coefficient α defined above. These approximations and their consequences are addressed in more detail further on.

2.2. *The Canonical Equations of Motion*

In all the rest of this paper, we consider the *planar* problem; i.e., we assume that the grain and the planet orbit in the same plane. The gravitational forces are classically derived from the conservative potential of the system. Therefore, the motion of the dust grain is described by

$$\ddot{\eta}_j = \frac{\partial U}{\partial \eta_j} + X_j(\zeta), \tag{6}$$

where η_1, η_2 are the grain Cartesian coordinates in the plane of the planetary orbit, U is the negative of the potential energy, and $X_j(\zeta)$ takes into account the nonconservative effect of the PR drag, as given by (5).

Introducing the associate momenta,

$$\zeta_j = \dot{\eta}_j, \tag{7}$$

we can write the canonical system,

$$\begin{aligned} \dot{\zeta}_j &= \frac{\partial F}{\partial \eta_j} + X_j(\zeta) \\ \dot{\eta}_j &= -\frac{\partial F}{\partial \zeta_j}, \end{aligned} \tag{8}$$

the Hamiltonian being

$$F = -\frac{1}{2}\sum_{j=1}^{2}\zeta_j^2 - U(\eta)$$

$$U = \frac{\mathcal{G}(M_\star + m_g)}{r_g} + \mathcal{G}m_p\left(\frac{1}{r_{gp}} - \frac{\mathbf{r}_g\cdot\mathbf{r}_p}{r_p^3}\right).$$

In this expression, as throughout the present paper, the subscript "g" refers to the dust grain, while "p" refers to the planet. The vector $\mathbf{r}$ defines the position of a point from the star center, and r_{gp} stands for the modulus of $\mathbf{r}_g - \mathbf{r}_p$, while m represents a mass.

As we are interested in the combined effects of first order resonances and Poynting–Robertson drag, we follow the procedure introduced by Ferraz-Mello (1992) and canonically transform the above system to more suitable variables. A lemma from Brouwer and Hori (1961) for systems with a dissipative term ensures the canonicity of the transformations. Considering the planar problem we perform three variable transformations,

$$(\eta_1, \eta_2, \zeta_1, \zeta_2)$$
$$\Downarrow$$
Delaunay variables $(L, G, \lambda_g, \tilde{\omega}_g)$
$$\Downarrow$$
Extended phase space $(L, G, \Lambda, \lambda_g, \tilde{\omega}_g, t)$
$$\Downarrow$$
Resonance variables $(J_1, J_2, J_3, \theta_1, \theta_2, \theta_3)$,

where a_g, e_g, λ_g, $\tilde{\omega}_g$ are the classical orbital elements, i.e., the semimajor axis, eccentricity, mean longitude, and longitude of the pericenter, respectively. The Delaunay variables are defined by

$$L = \sqrt{\mu a_g} \quad G = L\sqrt{1 - e_g^2}$$

with $\mu = \mathcal{G}(m_g + M_\star)$. The variable Λ is the conjugate of the time t and the resonance variables are defined as

$$J_1 = L - G \qquad \theta_1 = (q+1)\lambda_p - q\lambda_g - \tilde{\omega}_g$$
$$J_2 = \frac{n_p G + \Lambda}{n_p - f_p} \qquad \theta_2 = (q+1)\lambda_p - q\lambda_g - \tilde{\omega}_p$$
$$J_3 = (q+1)L + q\frac{f_p G + \Lambda}{n_p - f_p} \qquad \theta_3 = \lambda_g - \lambda_p,$$

where n_p and f_p are the planetary mean motion and the precession of the pericenter, respectively, considered as constants. Finally, q is an integer defining the first order resonance $(q+1):q$; i.e., we investigate the motion of the grain for

$$(q+1)n_p - qn_g \sim 0.$$

In our problem, the planetary orbit is interior to that of the dust grain, so that q will always be *negative*.

We will not enter in the details of these transformations, since they are analogous to those given by Ferraz-Mello (1992) and Beaugé and Ferraz-Mello (1993). It must just be noted here that the Hamiltonian is considered in the form

$$F = \frac{\mu^2}{2L^2} - \Lambda + R, \tag{9}$$

where R is the perturbing function in which we keep only the constant, secular, and resonant terms. We adopt for R the classical expansion in the Laplace coefficients and in powers of the eccentricities,

$$R = \frac{\mathcal{G}m_p}{2}\left[A_{pg}^0 + \frac{1}{4}B_{pg}^1(e_p^2 + e_g^2)\right.$$
$$-\frac{1}{2}e_p e_g B_{pg}^2\cos(\theta_1 - \theta_2) - D_{pg}e_g\cos\theta_1 \tag{10}$$
$$\left. + M_{pg}^q e_p\cos\theta_2 - \frac{a_g e_g}{a_p^2}\delta^q\cos\theta_1\right],$$

with

$$D_{pg}^{q+1} = \frac{1}{a_g}\left\{(2q+1)b_{1/2}^{q+1} - \xi\frac{db_{1/2}^{q+1}}{d\xi}\right\}$$
$$M_{pg}^q = \frac{1}{a_g}\left\{2qb_{1/2}^q - \xi\frac{db_{1/2}^q}{d\xi}\right\}$$
$$A_{pg}^0 = \frac{1}{a_g}b_{1/2}^0 \tag{11}$$
$$B_{pg}^q = \frac{\xi}{a_g}b_{3/2}^q,$$

$b_s^q(\xi)$ being the classical Laplace coefficients with $\xi = a_p/a_g$. The δ^q in the last term of Eq. (10) stands for

$$\delta^q = \begin{cases} 1, & \text{if } q = -2; \\ 0, & \text{otherwise.} \end{cases}$$

This term comes from the indirect part of the perturbing function. In Eq. (10), secular terms are expanded up to e^2, while periodic terms are expanded up to e. This is a classical result of celestial mechanics, which stems from the fact their effects on the motion are of the same order.

As we shall see, the coefficient D_{pg}^{q+1} will always appear as a multiplicative factor together with the mass m_p of

the planet. This factor actually scales the strength of the forcing term acting on the orbital eccentricity of the grain. For order of magnitude calculations, it will be useful to express D_{pg}^{q+1} in the form

$$D_{pg}^{q+1}(\xi) \equiv \frac{f(q)q}{a_g}. \tag{12}$$

This defines the function f, which is usually of order unity, and which depends *weakly* on q. Near a resonance, $(q+1)n_p - qn_g \sim 0$, so that Kepler's third law yields $\xi \sim (1-\beta)^{-1/3}[(q+1)/q]^{2/3}$. The term in $1-\beta$ takes into account the reduction of the mass of the central star as perceived by the grain. The value of D_{pg}^{q+1} is then calculated by introducting the value of ξ in the first Eq. (11), and by using the usual expansions of the Laplace coefficients. For $\beta = 0$, the factor f is ~1.69 ... for $|q| = 2$ (1:2 resonance), and tends to 1.60 ... as $|q|$ tends to infinity. When β is nonzero, the situation is more complicated because a resonant radius will coincide with the planet orbital radius, leading to the divergence of f. This does not occur in our present study because we use only small values of $|q|$ (typically 2 to 5) and β (0.3 at most). For instance, with $\beta = 0.3$, f varies from 2.14 ... for $|q| = 2$ to 6.71 ... for $|q| = 5$. Consequently, in this paper, the value of f will always be in the range ~2–6.

It must be noted that the equations hereafter derived *are valid only for small eccentricities*. We could have used an expansion which would account also for greater eccentricities, such as the asymmetric expansion given by Ferraz-Mello (1987), but we have noted in our integrations that the crossing of a resonance (without capture) always occurs below an eccentricity e of about 0.07. If the grain remains in the resonance beyond this value, then it remains there for a long time, and escapes only when its orbital eccentricity is so high that it can have a close encounter with the planet (see Paper I). Note that in the remainder of this paper, we reserve the term "escape" for the latter phenomenon, while the term "noncapture" or "crossing of the resonance" refers to the passage through the resonance, even though a short time may be spent in that resonance.

Since we are essentially interested here in the mechanism of capture into a resonance, i.e., in the case $e \lesssim 0.07$, we will use the perturbing function R as defined by Eq. (10) in our calculations. Comparison with the integration of the exact equations of motion shows that this approach is actually valid (see Section 4.3 and Fig. 3).

The equations obtained are then averaged over the short period terms, θ_3. Introducing the nonsingular variables

$$H = \sqrt{2J_1}\sin\theta_1 \quad K = \sqrt{2J_1}\cos\theta_1, \tag{13}$$

we finally obtain

$$\begin{aligned}
\dot{H} &= AK - BR_K - \frac{\alpha}{2}H[1 + 4LCB^2] \\
\dot{K} &= -AH + BR_H - \frac{\alpha}{2}K[1 + 4LCB^2] \\
\dot{\theta}_2 &= S_1 - f_p \\
\dot{J}_2 &= -\frac{\mathcal{G}m_p}{2}\left[\left(M_{pg}^q - \frac{1}{2}BKB_{pg}^2\right)e_p\sin\theta_2 \right. \\
&\qquad \left. + \frac{1}{2}BHB_{pg}^2 e_p\cos\theta_2\right] - \frac{\alpha(L-J_1)}{1-\gamma} \\
\dot{J}_3 &= -\frac{\alpha}{1-\gamma}[(q+1-\gamma)(2C-1)L - \gamma q J_1(1+4LCB^2)],
\end{aligned} \tag{14}$$

where

$$\gamma = \frac{f_p}{n_p}$$

$$A = S_1 + \frac{KR_K + HR_H}{4BL^2}$$

$$S_1 = [(q+1)n_p - qn_g] - (KR_K + HR_H)\frac{\partial B}{\partial J_2} + \frac{2qL}{\mu}R_a$$

$$R_K = \frac{\mathcal{G}m_p}{2}\left\{\frac{1}{2}B_{pg}^1 BK - D_{pg}^{q+1} - \frac{1}{2}B_{pg}^2 e_p\cos\theta_2 - \frac{a_g}{a_p^2}\delta^q\right\}$$

$$R_H = \frac{\mathcal{G}m_p}{4}\{B_{pg}^1 BH - B_{pg}^2 e_p\sin\theta_2\}$$

$$B = \sqrt{\frac{1}{L} - \frac{J_1}{2L^2}}$$

$$C = \left(\frac{L}{L-J_1}\right)^2$$

$$R_a = \frac{\partial R}{\partial a_g}.$$

The above equations describe the planar motion of a dust grain near a $(q+1):q$ mean motion resonance. This system has two degrees of freedom, associated with two different kinds of resonances.

One degree of freedom is associated with (θ_1, J_1), or equivalently, with (K, H). For small eccentricities, we note that $K \sim (\mu a_g)^{1/4} e_g\cos(\theta_1)$ and $H \sim (\mu a_g)^{1/4} e_g\sin(\theta_1)$. Since a_g is nearly constant once the grain is trapped into the resonance, this means that the vector defined by (K, H) has a modulus proportional to e_g and a position angle given by the critical argument θ_1. For short, we will refer to (K, H) as the "eccentricity vector" (although a rigorous definition would require that the modulus of (K, H) be equal to e_g). Finally, the resonance associated with this

degree of freedom is referred to as a "Lindblad" resonance.

The other degree of freedom is associated with (θ_2, J_2). The variations of the action J_2 are driven by the planet orbital eccentricity e_p. The corresponding resonance is referred to as a "corotation" resonance. We refer the reader to Lissauer (1985), Goldreich *et al.* (1986), and Sicardy (1991) for a discussion of the physical differences between these two kinds of resonances. Briefly speaking, a Lindblad resonance can force large excursions of the grain's orbital eccentricity, while a corotation resonance is able to trap θ_2 in finite libration motion, causing the grain to librate also in finite intervals of longitude, but keeping the eccentricity e_g essentially unchanged. The confinement of material in longitude (or arcs) due to corotation resonances is illustrated in Paper 1 and in Patterson (1987).

In this paper, we are mainly interested in better understanding the simpler problem of a grain perturbed by PR drag and by a planet in a *circular* orbit ($e_p = 0$) with no precession ($\gamma = 0$). In the absence of any further information on possible planets associated with circumstellar disks, this is a reasonable first step. The full system (14) can nevertheless be used in general problems with dissipation, in which the grain is perturbed by a body in an eccentric orbit. The dissipation term (5) is sufficiently general so that a variety of problems relevant to the solar system can be treated.

With $e_p = 0$ and $\gamma = 0$, the system (14) reduces to

$$\begin{aligned}
\dot{H} &= AK - BR_K - \frac{\alpha}{2}H[1 + 4LCB^2] \\
\dot{K} &= -AH + BR_H - \frac{\alpha}{2}K[1 + 4LCB^2] \qquad (15) \\
\dot{J}_2 &= -\alpha(L - J_1) \\
\dot{J}_3 &= -\alpha(q + 1)(2C - 1)L.
\end{aligned}$$

3. BEHAVIOR OF THE SOLUTION NEAR A FIRST ORDER RESONANCE

3.1. Simplified Equations of Motion

In this paper, the system (15) is numerically integrated to study the capture of a grain into a resonance. During this integration, the variations of all the terms depending on the particle semimajor axis are taken into account. An intuitive behavior of the solution is then difficult to derive. However, when the particle's orbital eccentricity is still small, several simplifications are possible, and the qualitative behavior of the grain orbit may be more clearly understood.

Thus, assuming that $e_g \ll 1$ and $e_p = 0$, we have

$$\begin{aligned}
A &\sim S_1 \\
S_1 &\sim (q + 1)n_p - qn_g \equiv \Delta n \\
R_H &\sim 0 \\
R_K &\sim -\frac{\mathcal{G}m_p D_{pg}^{q+1}}{2} \qquad (16) \\
B &\sim \frac{1}{\sqrt{L}} \\
C &\sim 1.
\end{aligned}$$

The quantity Δn defined above is a measure of the "distance" from the particle to the exact resonance, where $\Delta n = (q + 1)n_p - qn_g = 0$. Near a resonance, and for small eccentricity, the quantity Δn depends only on a_g. The variation of Δn with time is derived from Kepler's third law, $a_g^3 n_g^2 =$ constant, thus $\Delta\dot{n} = 3qn\dot{a}_g/(2a)$. From $L = -q(J_1 + J_2) + J_3$ and the approximations (16), one finally gets the simplified equations of motion

$$\begin{aligned}
\dot{H} &= \Delta nK + \varepsilon D' - \tfrac{5}{2}\alpha H \\
\dot{K} &= -\Delta nH - \tfrac{5}{2}\alpha K \\
\Delta\dot{n} &= \frac{3q}{a_g^2}[-q(\dot{J}_1 + \dot{J}_2) + \dot{J}_3] \qquad (17) \\
\dot{J}_2 &= -\alpha L \\
\dot{J}_3 &= -\alpha(q + 1)L,
\end{aligned}$$

where $D' \equiv (a_g^2 n_g^{3/2} D_{pg}^{q+1})/2 = a_g n_g^{3/2} f(q)q/2$ is a constant factor and

$$\varepsilon \equiv m_p/M_\star \ll 1$$

is the (small) mass of the planet relative to the mass of the star. Note that because of the definition of f (Eq. (12)), D' is of order $a_g n_g^{3/2}$.

In the system (17), the quantities a_g and n_g are fixed to their values at the resonance, but of course not Δn. Since $2J_1 = H^2 + K^2$, this system is closed. We first study the conservative case; i.e., we make $\alpha = 0$. Then we are left with three differential equations involving H, K, and Δn. This describes a two-degree-of-freedom motion. In principle, there should be a fourth equation, i.e., $\dot{\theta}_2 = S_1 \sim \Delta n$, but since θ_2 decouples from the other equations, it is not considered here.

Far away from the resonance ($|\Delta n|$ large), the eccentricity vector (K, H) follows a circle centered on the forced eccentricity $(-\varepsilon D'/\Delta n, 0)$, with an angular velocity Δn. Close to the resonance ($\Delta n \sim 0$), there is a strong coupling between the variations of H and K and the variations of

Δn. This may change the sign of Δn and cause a libration motion of (K, H).

The system (17) is integrable, since it admits two integrals of motion

$$C_1 = 2(H^2 + K^2) + \frac{4a_g^2}{3q^2}\Delta n$$
$$C_2 = (H^2 + K^2)^2 - C_1(H^2 + K^2) - \varepsilon\frac{8D'a_g^2}{3q^2}K. \quad (18)$$

The motion of (K, H) can be visualized by defining a 3D space, composed of a "horizontal" plane OKH where the eccentricity vector evolves, and a "vertical" axis OZ (Fig. 1a). The following discussion is derived from the analysis of Ferraz-Mello (1985), who gives a thorough morphogenetic analysis of the motion of the eccentricity vector at a first order resonance. The conservation of C_1 and C_2 implies that the trajectory of (K, H) is the projection onto the horizontal plane of two surfaces in the 3D space $OKHZ$. One surface, M, is defined by $Z = (H^2 + K^2)^2 - C_1(H^2 + K^2)$ and is vertically axisymmetric. If $C_1 \leq 0$, this surface has only one minimum, at $H = K = 0$. If $C_1 \geq 0$, it has one maximum ($K = H = 0$), and reaches a minimum value along the circle $H^2 + K^2 = C_1/2$. The surface M is then referred to as a "Mexican hat" surface (Figs. 1a and 1b).

The other surface, P, is defined by $Z = C_2 + \varepsilon 8D'a_g^2/3q^2K$; it is thus a plane parallel to the H axis. It has a (small) slope $\varepsilon 8D'a_g^2/3q^2$ with respect to the horizontal plane OKH. This plane is shown in dashed lines in Fig. 1a. The intersections of the two surfaces M and P with the OKZ plane are drawn in Fig. 1b. If C_1 is positive, the trajectory of (K, H) can be in three different zones, depending on the value of C_2. For large eccentricities, only external circulations are possible. Near the origin O, we have inner circulations, while in the intermediate region, (K, H) is trapped in a libration motion around L. Each kind of trajectory, projected onto the OKH plane, is sketched in Fig. 2a.

3.2. *Effect of Dissipation*

We now analyze the dissipative problem ($\alpha > 0$). We calculate the derivatives of C_1 and C_2 by introducing their expressions (18) in the system (17). Then

$$\dot{C}_1 = -\frac{4\alpha a_g^2 n_g}{q}$$
$$\dot{C}_2 = \frac{4\alpha a_g^2 n_g}{q}(H^2 + K^2). \quad (19)$$

It is easy to show that the minimum value of Z on the Mexican hat surface is $Z_{min} = -C_1^2/4$ (Fig. 1b). Consequently, the dissipation causes a variation of Z_{min} at the rate $\dot{Z}_{min} = -C_1\dot{C}_1/2 = 2\alpha C_1 a_g^2 n_g/q$. Note that because $q \leq 0$, Z_{min} is steadily decreasing. Finally, near the libration point L, we have $H^2 + K^2 \sim C_1/2$, and thus, from the second Eq. (19),

$$\dot{Z}_{min} \sim \dot{C}_2. \quad (20)$$

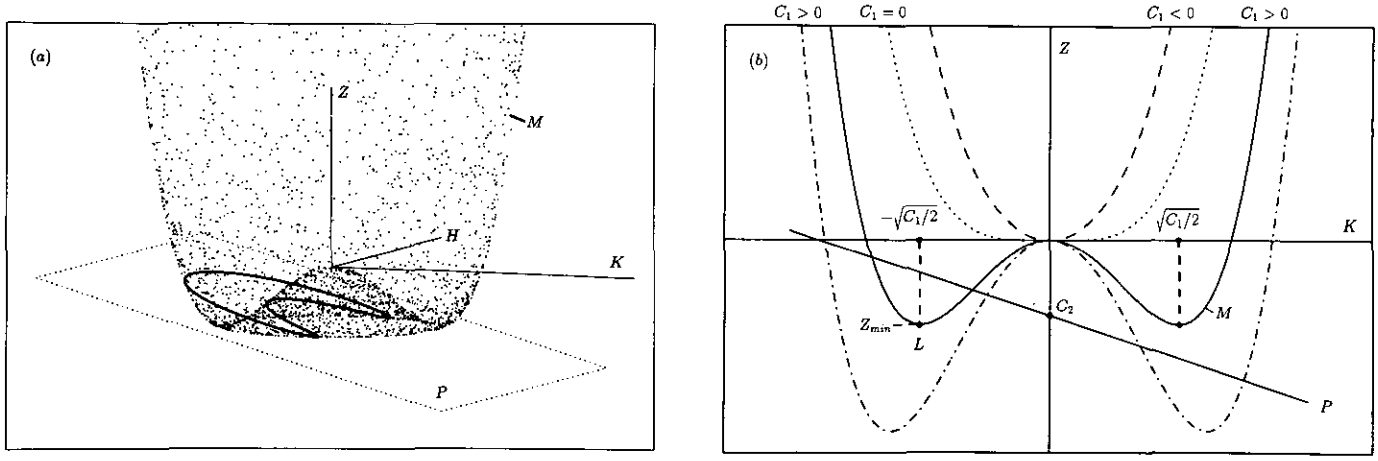

FIG. 1. (a) A 3D view of the "Mexican hat" surface M and the intersecting plane P (dashed line). Points have been scattered randomly on the Mexican hat surface for a better visualization of the 3D surface. The solid, bean-shaped curve is the intersection of the two surfaces. It represents the trajectory followed by the eccentricity vector in the conservative case. See the text for details. (b) Lateral view of Fig. (a), with the projection of various Mexican hat surfaces onto the OKZ plane. The tilted straight line is the projection of the plane P defined in (a). Before the entrance into the resonance ($C_1 < 0$), M has only one minimum, at O. At the entrance into the resonance ($C_1 = 0$), the surface flattens. After a while ($C_1 > 0$, see the solid line), two minima have appeared. Their ordinates Z_{min} decrease at the same rate as C_2 (Eq. (20)). Later on, the minima are more pronounced (dashed–dotted line); the forced eccentricity $-\sqrt{C_1/2}$ continues to shift to the left.

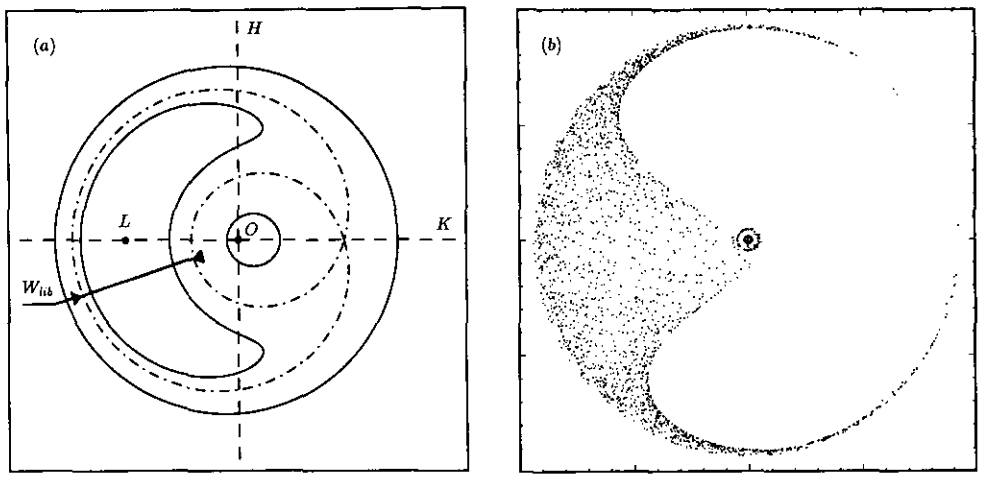

FIG. 2. (a) Various intersections, projected onto the OKH plane, of the surface M shown in Fig. 1a with different planes P. Two circulating (internal and external) trajectories are drawn. The librating, bean-shaped libration trajectory is the same as the one shown in Fig. 1a. The dashed–dotted line is the separatrix between the various regimes. (b) Evolution of the eccentricity vector (H, K) for high eccentricities, obtained by integrating the system (15) near a 3:4 resonance, with $\beta = 0.3$. The latter corresponds to a particle radius of ~2.7 μm (in the geometrical approximation) orbiting β Pictoris. Note the asymmetrical libration near 180° caused by dissipation. The escape from the resonance occurs near the equilibrium eccentricity defined by Eq. (28). Units are arbitrary in both panels.

This equality has an important consequence, since it ensures that the minimum value on the Mexican hat surface, and the intersecting plane P moves downward at the *same* rate.

The general scenario of capture into a resonance may be then understood as follows: (i) Suppose that a particle is well outside the resonance, on a circular orbit ($K = H = 0$); then $\Delta n < 0$ and also $C_1 < 0$. The first Eq. (19) shows that, because of dissipation, C_1 increases at a constant rate $-4\alpha a_g^2 n_g/q$, since q is negative. During this time, C_2 remains constant because $K = H = 0$, according to the second Eq. (19); thus the intersecting plane P does *not* move. (ii) When the resonance is reached, C_1 becomes positive. Two shallow minima appear on the curve $Z = K^4 - C_1K^2$ (Fig. 1b, curve labeled $C_1 = 0$). Simultaneously, the intersecting plane starts moving downward at the same rate as Z_{min}, provided that the eccentricity vector remains close to the libration point L. (iii) This synchronization derived in Eq. (20) makes the capture into the resonance possible, since (K, H) remains in the libration region near L. (iv) The eccentricity corresponding to libration point L is $e_{lib} = \sqrt{C_1/2}/(a_g n_g^{1/2})$. Because C_1 is a linear function of time (Eq. 19), we have

$$e_{lib} = \sqrt{(2\alpha/|q|)t}, \tag{21}$$

where the time t is counted from the entrance into the resonance. (v) Since L corresponds to $H^2 + K^2 = C_1/2$, it also corresponds to $\Delta n = 0$, according to Eq. (18). Thus, the semimajor axis of the particle remains fixed at the resonant radius. This scenario explains the main features observed during the numerical integrations: in a first stage, the semimajor axis of the grain decreases, while the eccentricity remain close to zero. When the resonance is reached, the semimajor axis is locked at a fixed value, corresponding to $\Delta n \sim 0$, while the eccentricity increases like $\sqrt{t}$.

It is interesting to note, from Eq. (21), that the typical time scale for increasing significantly the eccentricity is $\sim|q|/\alpha$. On the other hand, Eq. (5) shows that the time scale for orbital decay due to PR drag is of order $1/\alpha$. This means that, when effective, the trapping occurs on time intervals long enough to statistically accumulate the particle semimajor axes at the resonance radii.

3.3. *Nonadiabaticity of the Motion*

A difficulty arises at that point. Our analysis does not take into account the phase θ_1 of the eccentricity vector (K, H). Rather, we assume that the dissipation is small enough so that C_1 and C_2 vary very slowly, and an adiabatic invariant analysis can be applied. Namely, we consider that the changes of the phase space topology induced by the changes of C_1 and C_2 are small enough to preserve the area enclosed inside the trajectory of (K, H). We shall see that this is *not* the case, or only marginally, for typical circumstellar grains around a star such as β Pictoris. In this case, and especially when the two minima shown in Fig. 1b are still very shallow (entrance into the resonance), the phase θ_1 may be such that the vector (K, H) crosses the separatrix and escapes the resonance (see the example of Fig. 11). The nonadiabaticity of the motion makes the

estimate of the probability of capture a rather difficult task, so that we have to turn to numerical integration.

This nonadiabaticity may be quantified as follows. According to (21), the eccentricity $e_{\rm lib}$ corresponding to the stable libration point L (Fig. 2a) changes at the rate

$$\dot{e}_{\rm lib} = -\frac{\alpha}{q e_{\rm lib}}. \tag{22}$$

Considering that the slope of the oblique straight line P in Fig. 1b is small, one easily shows that the width $w_{\rm lib}$, in eccentricity, of the libration zone is (see Fig. 2a)

$$w_{\rm lib} = \sqrt{\left(\frac{16}{3q^2}\right)\left(\frac{\varepsilon}{e_{\rm lib}}\right)\left(\frac{|D'|}{a_{\rm g} n_{\rm g}^{3/2}}\right)}. \tag{23}$$

The topology of the phase space will have suffered a significant change when the bean-shaped libration zone has moved by its own width. The typical time scale of significant evolution for the phase space is thus $T_{\rm evol} \sim w_{\rm lib}/\dot{e}_{\rm lib}$; i.e.,

$$T_{\rm evol} \sim \frac{1}{\alpha}\sqrt{\frac{16}{3}\left(\frac{|D'|}{a_{\rm g} n_{\rm g}^{3/2}}\right)\varepsilon e_{\rm lib}}. \tag{24}$$

On the other hand, the typical libration period $T_{\rm lib}$ of the eccentricity vector around L is obtained by linearizing the system (17) near L. This yields

$$T_{\rm lib} \sim \frac{4T_{\rm orb}}{3|q|}\sqrt{\frac{3 a_{\rm g} n_{\rm g}^{3/2}}{16\varepsilon e_{\rm lib}|D'|}}, \tag{25}$$

where $T_{\rm orb}$ is the orbital period of the grain. The evolution of the (K, H) vector is thus adiabatic if $T_{\rm lib} \ll T_{\rm evol}$, i.e., if

$$\frac{T_{\rm lib}}{T_{\rm evol}} \sim \left(\frac{\alpha T_{\rm orb}}{2f|q|^2}\right)\left(\frac{1}{\varepsilon e_{\rm lib}}\right) \ll 1. \tag{26}$$

The value of $T_{\rm lib}/T_{\rm evol}$ will be estimated in Section 4 for typical grains around a star such as β Pictoris.

3.4. *Stationary Solution*

The numerical integration is also useful at the other end of the particle evolution, i.e., when the orbital eccentricity $e_{\rm g}$ is too high for the system (17) to be valid. Then we have to turn back to the system (15), where all the coefficients other than α and q vary at the same time, making an analytical study of this system difficult. Nevertheless, the question of the fixed points of this system can still be investigated. We use for that the more physical quantities $e_{\rm g}$, θ_1, and $L = \sqrt{\mu a_{\rm g}}$ instead of H, K, J_1, and J_2. Then the system (15) turns into

$$\begin{aligned}
\dot{L} &= -\frac{\mu}{2} q D_{\rm gp}^{q+1} \varepsilon e_{\rm g} \sin\theta_1 + \alpha L\left(1 - \frac{2}{\rho^2}\right) \\
\dot{e}_{\rm g} &= \frac{\mu}{2L}\varepsilon\rho(q + 1 - q\rho) D_{\rm pg}^{q+1} \sin\theta_1 - 2\alpha e_{\rm g} \\
\dot{\theta}_1 &= \Delta n - \frac{\mu}{4L}\frac{\varepsilon\rho(q+1-q\rho)}{e_{\rm g}} \\
&\quad \times [e_{\rm g} B_{\rm gp}^1 - 2D_{\rm pg}^{q+1}\cos\theta_1] + \frac{2qL}{\mu} R_{\rm a},
\end{aligned} \tag{27}$$

where we write for short $\rho = \sqrt{1 - e_{\rm g}^2}$. Note that the system above is no longer canonical.

The physical interpretation of the first two equations is the following. The dissipation damps the semimajor axis and the eccentricity of the grain, since the two terms containing α are negative. On the other hand, the resonance can provide energy through the terms containing $\sin\theta_1$. Because q and $D_{\rm pg}^{q+1}$ have the same sign, the first equation shows that energy can be provided to the grain only if $\sin\theta_1 < 0$. The second equation then shows that the eccentricity is *increased* by *outer* Lindblad resonances ($D_{\rm pg}^{q+1} < 0$) and *damped* by *inner* Lindblad resonances ($D_{\rm pg}^{q+1} > 0$). Thus only outer Lindblad resonances are able to counteract the dissipative effect of PR drag, i.e., are able to yield $\dot{e}_{\rm g} = 0$.

This result is a particular case of a more general phenomenon, the "shepherding mechanism," which tends to push the particle away from the planetary orbit as soon as some collective or irreversible effects are introduced in the system (see the reviews by Goldreich and Tremaine 1982 and by Meyer-Vernet and Sicardy 1987).

The equilibrium orbit is obtained by setting all the time derivatives to zero. Some simple algebra using the first two equations yields

$$\begin{aligned}
(q+1)(1+e_{\rm eq}^2) &= q(1-e_{\rm eq}^2)^{3/2} \\
\sin\theta_1 &= -\left(\frac{2L}{q\mu D_{\rm pg}^{q+1}}\right)\left[\frac{(1+e_{\rm g}^2)}{e_{\rm g}(1-e_{\rm g}^2)}\right]\left(\frac{\alpha}{\varepsilon}\right).
\end{aligned} \tag{28}$$

The equilibrium value $e_{\rm eq}$ can be extracted numerically from the first equation; the second equation then yields $\sin\theta_1$. Finally, Δn is derived from the last equation in (27). For this equilibrium orbit, the energy dissipated by the PR drag is exactly compensated for by the energy provided by the planet. The following conclusions can be driven from the last two sets of equations:

• Only external Lindblad resonances allow the existence of equilibrium orbits, according to the first Eq. (28) (which requires that $q \leq 0$).

• The second Eq. (28) requires that $\sin\theta_1 \leq 0$, i.e., $\pi \leq \theta_1 \leq 2\pi$. Equivalently, the particle must have a conjunction with the planet after it has passed its apoapse, but before it has reached its periapse. This is a very general result, which ensures that the satellite *provides* energy to the particle to counteract the effect of dissipation (see the discussions by Peale 1976, Weidenschilling and Davis 1985, Jackson and Zook 1989, and Sicardy *et al.* 1993). This also has an important consequence for the orientation of the particle orbits in a frame corotating with the planet; see Paper 1.

• For large $|q|$'s, an approximate value of e_g at equilibrium is

$$e_{eq} \sim \frac{1}{\sqrt{2.5|q|}}. \tag{29}$$

One notes that this equilibrium eccentricity is *independent* of the damping coefficient. The above value is the same as the equilibrium eccentricity derived by Weidenschilling and Jackson (1993) and discussed by Sicardy *et al.* (1993) in the case of PR drag. A similar expression was derived by Weidenschilling and Davis (1985) and by Beaugé and Ferraz-Mello (1993) in the case of gas drag. In this case, however, the value of e_{eq} depends *also* on $\Delta V/V_K$, the relative deviation of the gas velocity from Keplerian motion. This difference arises from the fact that the friction against the gas is proportional to the relative velocity between the body and the gas, whose orbital velocity is itself close to the Keplerian velocity. In contrast, the PR drag is directly proportional to the orbital velocity of the body, as seen in Eq. (5).

• Substituting the equilibrium value obtained in (29) into (28), one obtains

$$\sin\theta_1 = -\left(\frac{2\sqrt{2.5}L}{|q|^{1/2}\mu D_{pg}^{q+1}}\right)\left[\frac{(2.5|q|+1)}{(2.5|q|-1)}\right]\left(\frac{\alpha}{\varepsilon}\right). \tag{30}$$

Thus, the equilibrium requires that the ratio α/ε be smaller that a limiting value imposed by the condition $|\sin\theta_1| \leq 1$. Physically, this means that if the dissipation is too strong, or if the planetary mass is too small, not enough energy is provided to the grain, even for $\theta_1 = -\pi/2$. We shall estimate the typical limiting value of ε, once some typical values of α relevant to circumstellar disks have been fixed. We shall see that this limiting value falls into the range of usual planetary masses.

The stability of the equilibrium orbit is a much more difficult matter. The analysis of the eigenfrequencies of the system (17) near the fixed point shows that the latter is stable (Beaugé and Ferraz-Mello 1993, Sicardy *et al.* 1993). However, in the more correct system (15), all the coefficients depending on a_g vary, and the linear stability of the equilibrium is no longer warranted. Again, a numerical integration is most useful for investigating this point.

In typical runs, the eccentricity does reach a maximum value corresponding to the value given by Eq. (29). At that point, the value of e_g remains almost constant with time, while the eccentricity vector exhibits a libration motion with larger and larger amplitude (Fig. 2b). Eventually, the separatrix is crossed, and the particle suddenly escapes the resonance region. This behavior is common to all the integrations that we have performed, either averaged as in system (15), or exact as in Paper 1. Actually, *none* of the orbits integrated on the Connection Machine in Paper I reaches a permanent equilibrium. This suggests that either the equilibrium orbits are not stable, or at least they are not attractors, for a wide range of initial conditions.

It is at present difficult to understand better the dynamics involved near equilibrium, since the system (15) is no longer valid at those eccentricities. Fig. 2b, however, suggests that the libration motion occurs in a more and more narrow region. This is expected also from Eq. (23), since it shows that w_{lib} decreases as e_{lib} increases. From Eq. (26), one can also conclude that the motion is more and more adiabatic as e_{lib} increases. This circumstances suggest that the conservation of the area enclosed in the librating trajectory forces the amplitude of the libration to increases as the width of the libration region shrinks. Direct integrations of the full problem could help solve this problem, which at present remains open (see also Paper 1 and Section 5.4).

4. NUMERICAL INTEGRATIONS

4.1. Choice of the Parameters

The system (15) is numerically integrated, using parameters and initial conditions compatible with the observations of the β Pictoris circumstellar disk (Smith and Terrile 1984, Artymowicz *et al.* 1989, and Paper 1). The particle radius s lies in the micrometer-sized range, the stellar mass $M_\star$ is estimated to 1.5 solar masses ($M_\odot$), and the stellar luminosity $L_\star$ is ~6 solar luminosity ($L_\odot$). We consider a planet orbiting at a_p = 20 AU, this distance corresponding to the estimated radius of the inner clearing zone of the disk. We also assume that the planet and the particle are moving in the same plane, the particle being launched at 30 AU.

The numerical integration of the system (15) is performed with a variable step size integrator, based on the Bulirsch–Stoer scheme (Bulirsch and Stoer 1966). The values of the coefficients α and β defined in Eqs. (2) and (4) are derived according to the work of Burns *et al.* (1979),

$$\beta \sim \left(\frac{0.2}{s_{\mu m}}\right)\left(\frac{L_\star}{L_\odot}\right)\left(\frac{M_\odot}{M_\star}\right)$$
$$\alpha \sim 1.2 \times 10^{-4}\left(\frac{L_\star}{L_\odot}\right)\left(\frac{1}{s_{\mu m} a_{AU}^2}\right) \text{year}^{-1}, \quad (31)$$

where $s_{\mu m}$ and a_{AU} are the particle radius in micrometers and the semimajor axis in AU, respectively. These estimations assume that the density of the particle is 3 g cm^{-3}, and that we are in the regime of geometrical optics (Q = 1). For particles around β-Pictoris, we thus have

$$\beta \sim \frac{0.8}{s_{\mu m}}$$
$$\alpha \sim \frac{7.2 \times 10^{-4}}{s_{\mu m} a_{AU}^2} \text{year}^{-1}. \quad (32)$$

The quantity α provides a rough estimate of the decay time of a particle due to PR drag: $t_{decay} \sim 1/\alpha \sim 1400 s_{\mu m} a_{AU}^2$ years. Therefore, at 20 AU, this decay time is of the order of 1 million years for micrometer-sized particles.

4.2. *Trapping into a Resonance*

An important restriction of the system (15) is that it is valid only *near* a first order resonance. However, as the grain crosses a resonance, and continues its decay towards the star, it is under the simultaneous influence of the resonance it has just crossed and the next resonance, not to mention higher order resonances. In the present paper, we are actually interested in the mechanisms of entrance into a first order resonance. Thus, we use only one resonant perturbing function R at a time (Eq. 10). Every time the particle goes out of the zone of influence of a resonance, and enters into the zone of influence of the next resonance, the value of R is changed accordingly. This abruptly modifies the coefficients in the system (15). More specifically, the change from the $(q + 1):q$ resonance to the adjacent $(q + 2):(q + 1)$ resonance is performed every time the relation

$$|(q + 2)n_p - (q + 1)n_g| < |(q + 1)n_p - qn_g| \quad (33)$$

is satisfied.

We could have used a smoother change of the parameters, but we know that the influence of a resonance becomes important only when the distance to it, Δn, approaches zero. Therefore, if we are interested only in the mechanism of capture into a given resonance, the above procedure is quite accurate. It must be kept in mind, however, that this procedure does not reproduce completely the integration of the exact equations of motion, since the orbital phase of a particle is an important parameter for its capture into a resonance. The integration of the exact equations of motion (Paper 1) also shows that particles can be trapped into higher order resonances, an effect not taken into account here.

We use the following nomenclature to describe the evolution of the grain near a resonance. The exact integrations of Paper 1 show that if the grain orbital eccentricity reaches the value of ~0.07, then it continues to increase toward the equilibrium value given by Eq. (29). In this case, we say that the grain is *trapped* into the resonance. This does not mean that this trapping is permanent, but rather that it occurs on time scales comparable to or larger than the decay time t_{decay} toward the star in the absence of the perturbing planet.

For eccentricities smaller than ~0.07, the particle may cross the separatrix enclosing the libration region shown in Fig. 2a, and then continue its decay toward the star. In this case, we say that the particle *crosses* the resonance.

The numerical integration is stopped in two cases: (i) when the semimajor axis of the grain reaches 21 AU, we consider that the grain has a close approach with the planet and is ejected from that region, or falls onto the star; (ii) when the eccentricity of the grain reaches 0.1, we consider that the grain is captured into the resonance and remains there for a long period. Also, the integration is not pursued because the system (15) is no longer valid for large eccentricities.

4.3. *Comparison with the Exact Equations of Motion*

In order to check whether the averaged system (15) adequately reproduces the mechanism of capture, we have integrated the exact equations of motion, all the physical parameters of the problem being equal. We recall here the main approximations made to obtain the averaged system (15):

- The dissipation coefficient α defined in Eq. (4) is assumed to depend only on a_g, while it actually depends on the averaged value of r^{-2}, and thus also on e_g. In other words, to calculate α, we consider that the eccentricity is zero, and we use $r = a_g$.
- The dissipative force associated to the radial term in Eq. (3) has been dropped. This assumes again that the orbit of the grain is circular.

To test the first assumption, we have integrated the system (15) with α constant, together with the exact equations of motion with α variable, but still dropping the radial term $-(\dot{r}/c)\mathbf{u}_r$ in Eq. (3). In Figs. 3a and b, the resulting eccentricity is plotted against the semimajor axis for each integration, respectively, with a planetary mass of 10^{-4} $M_\star$ and a value of β = 0.3, corresponding to a particle size of s = 2.7 μm (Eq. (32)). Otherwise, the initial orbital elements of the particle are the same. One

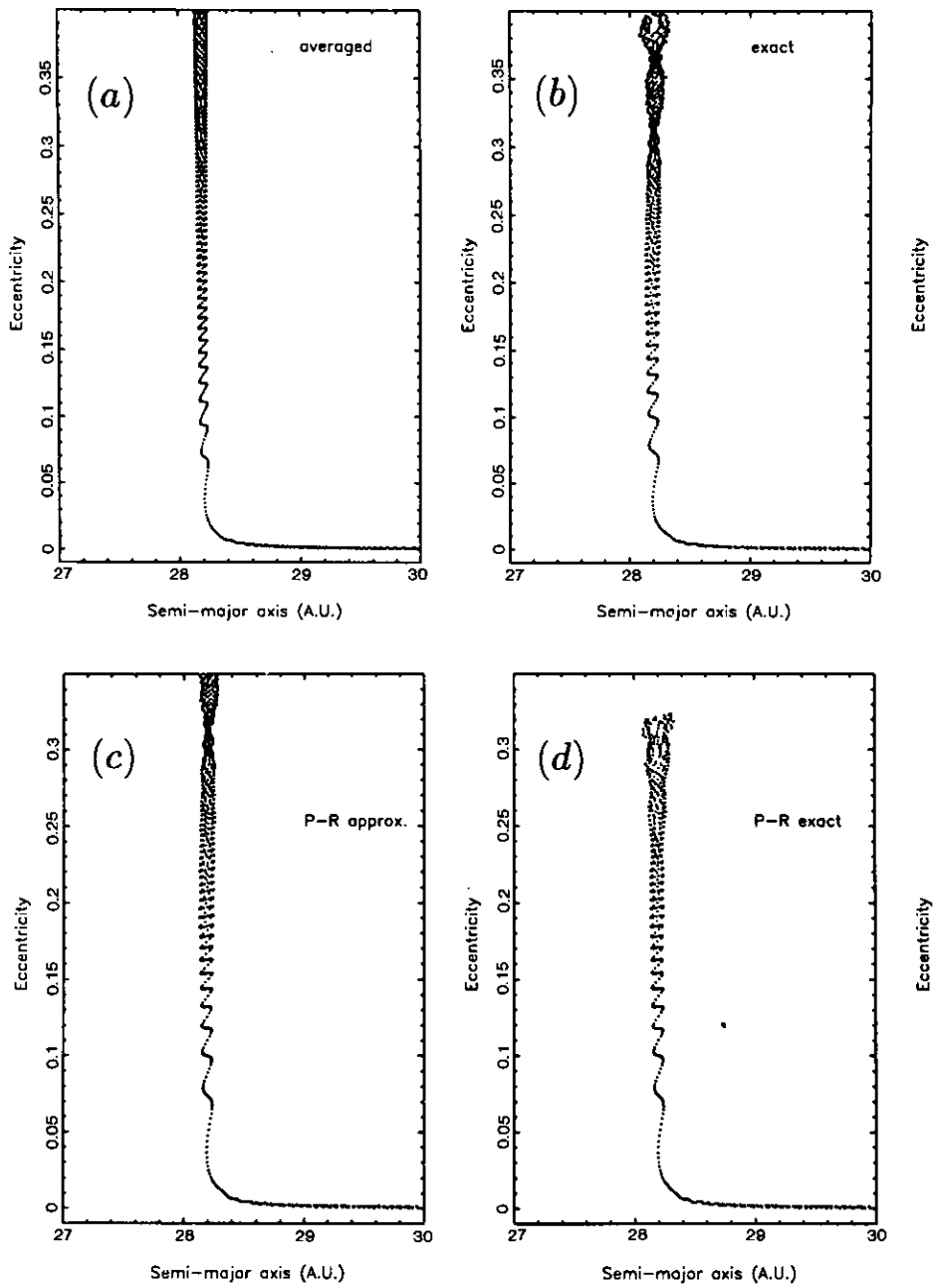

FIG. 3. The eccentricity vs the semimajor axis for a grain trapped in the outer 1 : 2 mean motion resonance. The planet is on a circular orbit around the star β Pictoris at a distance of 20 AU; its mass is $10^{-4}\ M_\star$ ($M_\star$ = mass of the star), or ~50 Earth masses, ~0.5 Saturn masses. The grain is initially released at 30 AU on a circular orbit. The coefficient β is 0.3. The points are plotted at intervals of 10 planetary revolutions, and the complete integration spans almost 1,000 planetary revolutions (a planetary revolution is about 73 years). (a) Result obtained by integrating the system (15), which assumes that the coefficient of dissipation α is constant along the orbit. (b) Integration of the exact equation of motion, taking into account the instantaneous value of α at each point of the orbit. (c) and (d) Comparison of the numerical integration of the exact equations of motion considering the tangent Poynting–Robertson (PR) drag only (c) and the total PR drag (d); see Eq. (3). Otherwise, the parameters used are the same as in (a) and (b). See the text for details.

can note the good agreement between the two integrations. Figures 3a and 3b show that the small oscillations in eccentricity start to be out of phase above $e_g \sim 0.1$, i.e., the value at which the numerical experiment is stopped. The integration of the averaged system (15) is about 20 times faster than the integration of the exact equations of motion.

To test the second assumption, we have integrated the

exact equations of motion, with the truncated dissipative force (Eq. 5), and then with the complete force given by Eq. (3). The results are plotted in Figs. 3c and 3d. We can see that the neglected terms are important only for high eccentricities, well above the limit of validity of our equations.

5. THE CAPTURE INTO A RESONANCE

5.1. *Influence of the Planetary Mass*

The masses chosen for the planets range from 5×10^{-6} to 10^{-4} stellar masses, $M_\star$, or equivalently, from ~2.5 Earth masses to ~0.5 Saturn masses.

A first question is the existence of equilibrium orbits, as defined by Eqs. (28). The first equation in this system yields the equilibrium value e_{eq}, which we will take equal to the value given in Eq. (29). Strictly speaking, this latter expression is valid for large $|q|$'s only, but this is good enough for the estimates that we make here. The second equation in (28) requires that $|\sin \theta_1| \leq 1$. Using the values of D_{pg}^{q+1} and α as defined in Eqs. (12) and (32), one gets the minimum mass necessary for equilibrium:

$$\varepsilon_{min} \sim \left(\frac{3.86 \times 10^{-4}}{f|q|^{3/2}}\right)\left(\frac{2.5|q|+1}{2.5|q|-1}\right)\left(\frac{\beta}{\sqrt{a_{AU}}}\right). \quad (34)$$

Choosing a typical value of $\beta = 0.3$, one gets values of ε_{min} in the range $\sim 4 \times 10^{-6}$ to 4×10^{-7} for $|q|$ in the range 2 to 5 (corresponding to ~2 to 0.2 Earth masses). This shows that the planets that we use in our integrations are in principle able to trap grains in equilibrium orbits. However, one should note here that the minimum mass defined by Eq. (34) is an *absolute* lower limit, since it assumes that the eccentricity has the equilibrium (maximum) value given by Eq. (29). As we shall see in Section 5.3, the very condition of capture at the *entrance* into the resonance, when the eccentricity is still small, is more complex than mere inequality $\varepsilon \geq \varepsilon_{min}$, and will require in general a larger mass than ε_{min} for the planet.

Figure 4 shows the evolution of a grain under the influence of planets with various masses and circular orbits ($e_p = 0$, $a_p = 20$ AU). The particle is initially released at 30 AU, also on a circular orbit. At time $t = 0$, the particle and the planet have the same longitude. The value of β is fixed to 0.3 in all these simulations. With this value, the resonances 1:2, 2:3, and 3:4 are located at 28.19, 23.27, and 21.51 AU, respectively. As the planet mass gets smaller, the grain crosses the first resonances, and is trapped in higher $|q|$ resonances. For a mass of about $5 \times 10^{-6}\ M_\star$, there exists no trapping at all. In Figs. 5a and 5b we show again the effect of the planetary mass, but now the particle is initially given a nonzero orbital eccentricity. We give here two examples, with initial eccentricities of 10^{-3} and 10^{-2} (5a and 5b, respectively). Even though the details of the evolution can be quite different, the main features of the capture/noncapture mechanism do not change. See, for example, the evolution through the 2:3 resonance for a planetary mass of $10^{-5}\ M_\star$. For small initial eccentricities (5a) we note an increase of eccentricity at the crossing of the resonance, while we have a decrease of eccentricity for larger initial eccentricities (5b). This point is discussed further in Section 5.4.

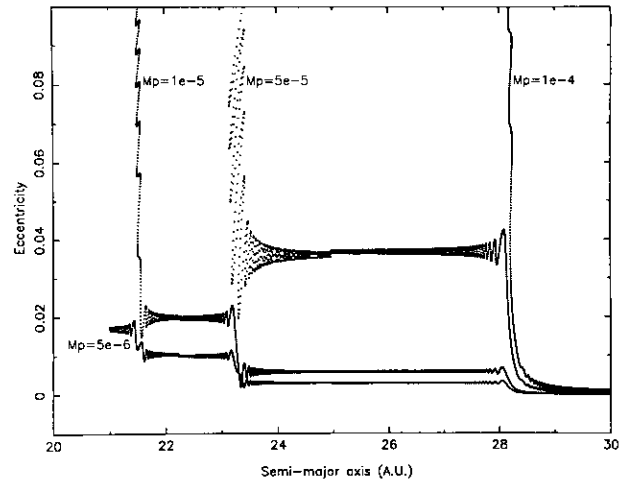

FIG. 4. Eccentricity of a grain vs its semimajor axis for different perturbing planetary masses. The system (15) is integrated using $\beta = 0.3$ and $e_p = e_g = \tilde{\omega}_p = \tilde{\omega}_g = \lambda_p = \lambda_g = 0°$ initially. The grain is released at 30 AU. The resonances 1:2, 2:3, and 3:4 are located at 28.19, 23.27, and 21.51 AU, respectively.

5.2. *Influence of the Dissipation Rate*

Changing α, or equivalently β, has two consequences. One is to change the time scale of evolution $1/\alpha$, larger particles evolving more slowly. A second consequence is to change the location of the resonance, since the radiation pressure modifies, by a factor of $1 - \beta$, the apparent mass of the star as perceived by the grain. Kepler's third law then implies that the resonance radius is multiplied by $(1 - \beta)^{1/3}$.

The influence of β is illustrated in Figs. 5c and 5d. In 5c, the value of β is fixed to 0.2 (particle radius ~4 μm), while the planetary mass is varied. One can note the great similarity of the particle behavior to that of Fig. 4. All our integrations actually show that the grain behavior, as far as the captured/noncapture mechanism is concerned, does not change for values of β between 0.1 and 0.3 (particle radius between 2.7 and 8 μm), confirming the results of Scholl *et al.* 1993, and of Paper 1. Figure 5d shows the effect of β, the mass of the planet being fixed to $5 \times 10^{-5}\ M_\star$. One can note the shift in radius of the 2:3 resonance location due to an increase of β.

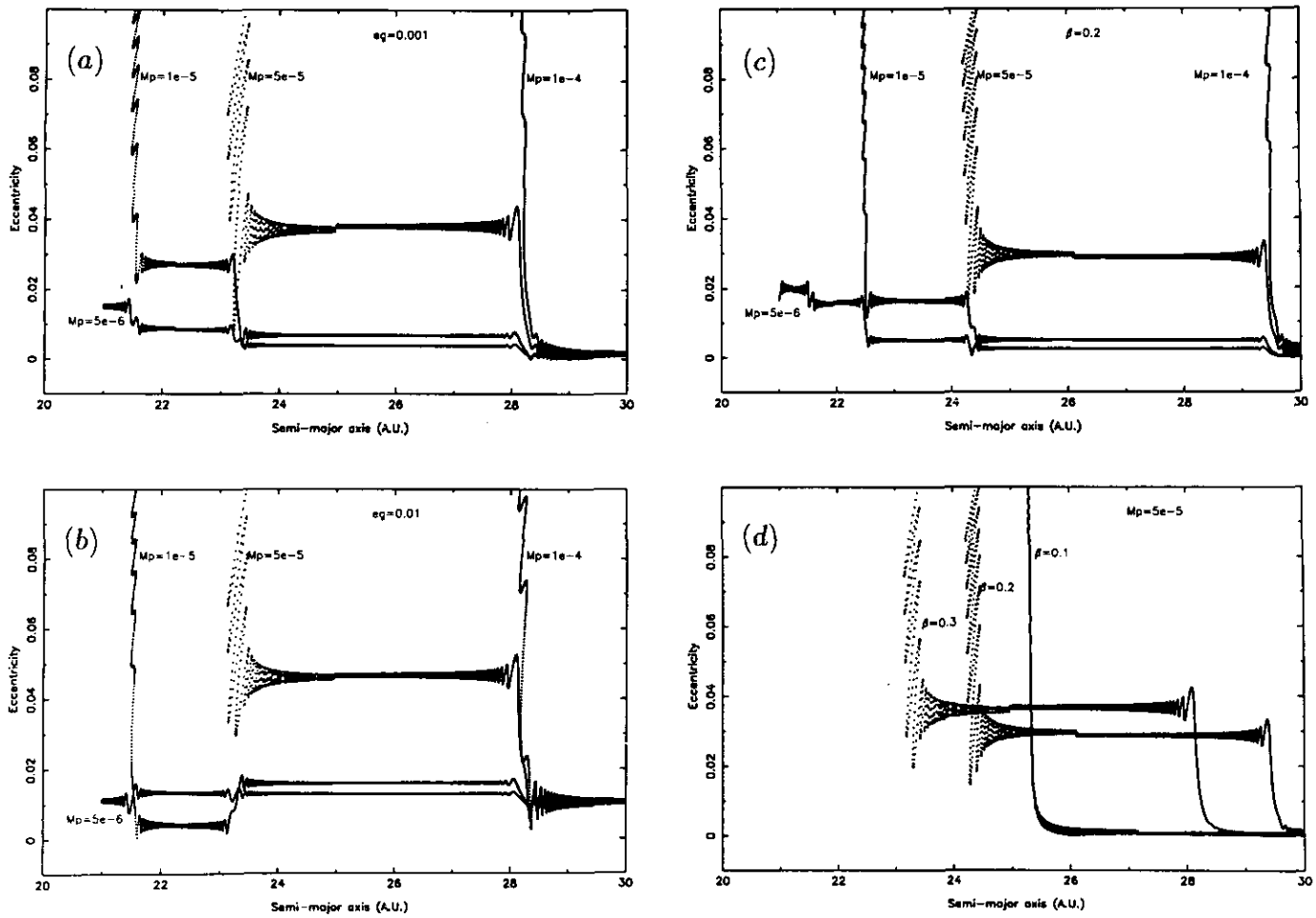

FIG. 5. The same as in Fig. 4, but with nonzero initial eccentricities for the grain: (a) initial eccentricity $e_g = 0.001$; (b) initial eccentricity $e_g = 0.01$; (c) the same as in Fig. 4, but with $\beta = 0.2$; (d) the planetary mass is $5 \times 10^{-5} M_\star$ (~25 Earth masses), and the value of β is changed from 0.1 to 0.3.

5.3. *Entrance into the Resonance*

Our analysis of the eccentricity vector behavior near a first order resonance (Section 3) provides the general scheme of the trapping mechanism. It fails, however, to give the probability of capture for particles whose orbital elements are randomly distributed. The main difficulty stems from the fact that the crossing of the resonance is nonadiabatic for typical particles under study.

Equation (26) gives the condition of adiabaticity of the motion. Using the parameters of β Pictoris, this equation reads

$$\frac{T_{\rm lib}}{T_{\rm evol}} \sim \left(\frac{3.83 \times 10^{-4}}{fq^2}\right)\left(\frac{\beta}{\sqrt{a_{\rm AU}}}\right)\left(\frac{1}{\varepsilon e_{\rm lib}}\right). \qquad (35)$$

The typical value of ε is 10^{-6}–10^{-5}, while $a \sim 25$ AU, $|q| = 2$ to 4, and $\beta \sim 0.3$. The value around which the eccentricity vector tries to oscillate at the entrance into the resonance is ~0.1 (see Fig. 11). Thus, Eq. (35) shows that the condition $T_{\rm lib}/T_{\rm evol} \ll 1$ is only marginally satisfied in most of our runs. Only for large, Jupiter-like planets ($\varepsilon \geq 10^{-4}$) and/or large grains (radius ≥ 10 μm) does the evolution become adiabatic. Examples of nonadiabatic evolutions are readily visible in Figs. 11 and 12: the eccentricity vector has no time to complete one libration cycle, while the libration point has moved significantly.

In fact, an important result derived from many integrations is that the resonance capture critically depends both on the eccentricity e_g of the grain at the entrance into the resonance, and on the resonant phase θ_1 at that moment.

For instance, we can fix the initial eccentricity and investigate the influence of θ_1. In practice, we change the initial longitude of the pericenter of the grain $\tilde{\omega}_g$, everything else being equal. We show in Fig. 6 an example with an initial eccentricity of 0.005. We note that the grain crosses the 1 : 2 resonance in all cases, and is trapped into the 2 : 3 resonance in three cases. Analyzing the eccentric-

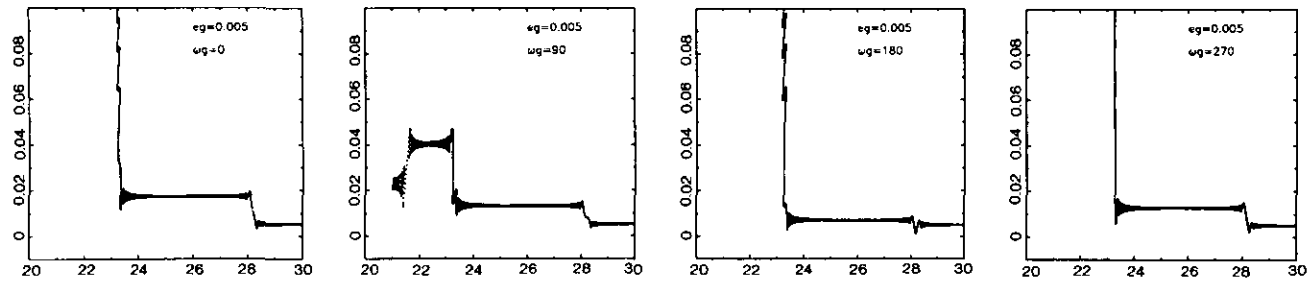

FIG. 6. The grain's eccentricity plotted against its semimajor axis (in AU). Each panel corresponds to a different initial argument of pericenter $\tilde{\omega}_g$ (in degrees), as indicated in the figure. The planetary mass is $2 \times 10^{-5} M_\star$ (~10 Earth masses), $\beta = 0.3$, and the initial eccentricity of the grain is 0.005.

ity variations as the grain crosses the 1 : 2 resonance, however, we note that it may have completely different behavior. We may observe an increase of eccentricity, a decrease, or no net change, even though there have been large variations during the crossing. This feature has been observed in all the tests performed.

A more compact form in which to present this study is to perform many integrations and plot the result of the resonance effect (capture or noncapture) in a grid, with the initial value of $\tilde{\omega}_g$ (corresponding to a value of θ_1) on one axis, and the initial value of e_g on the other axis. Such maps allow one to have a clearer idea of the probability of capture of the grain into a given resonance for a given planetary mass and a given value of β.

Examples of such a maps are shown in Figs. 7, 8, and 9, where the points (or the vertical bars) indicate a capture, as defined in Section 2.2. In the remaining regions, the particles cross the resonance. A quantity of interest is then the net jump in orbital eccentricity suffered by the grain, i.e., the eccentricity just after the crossing from the resonance minus the eccentricity just before the entrance into the resonance. The level curves link the points corresponding to a constant increase (solid lines) or a constant decrease (dashed lines) of the initial eccentricity after the crossing of the resonance.

Figures 7, 8, 9 correspond to the 1 : 2, 2 : 3, and 3 : 4 resonances, each panel showing the effect of a different planetary mass, keeping $\beta = 0.3$. In each resonance, the scenario is the same: a narrow tilted valley first appears when the planetary mass is increased, and this valley widens for small eccentricities, while the noncapture region shifts to the right. Note that the critical planet mass, for which the capture valley widens, is different from one resonance to the other: $7 \times 10^{-5} M_\star$ (~35 Earth masses) for the 1 : 2 resonance, $2 \times 10^{-5} M_\star$ (~10 Earth masses) for the 2 : 3 resonance, $10^{-5} M_\star$ (~5 Earth masses) for the 3 : 4 resonance.

One can note the smooth boundaries between the capture and noncapture regions, but also the absence of obvious symmetries or regularities in the shapes of these regions. We thus suspect that the shapes of these regions cannot be derived analytically. The main conclusions drawn from these maps may be summarized as follows:

- The trapping becomes more efficient as $|q|$ is increased. This can be expected from Eq. (28), since $\sin \theta_1 \propto 1/(qD_{pg}^{q+1}) \propto 1/q^2$. Thus the condition $|\sin \theta_1| \leq 1$ is more and more easily satisfied as $|q|$ is increased. Physically, this means that the strength of the resonance increases with $|q|$, everything else being equal.
- Roughly speaking, for planets with masses larger than ~1–5 $\times 10^{-5} M_\star$, and micrometer-sized particles, there are large regions of capture in the eccentricity–phase diagrams, provided the initial eccentricity of the grain is smaller than a few percent. This critical mass decreases as the q of the resonances is increased, from ~35 Earth masses for the 1 : 2 resonance to ~5 Earth masses for the 3 : 4 resonance. As expected, these masses are larger than the absolute minimum masses derived from Eq. (34), which yielded values ranging from ~2 Earth masses for the 1 : 2 resonance and ~0.2 Earth masses for the 3 : 4 resonance.
- More quantitatively, the maps yield the probability of capture in each case of interest, once an initial distribution of eccentricities and periapses has been specified.
- An analytical expression for the probability of capture may be difficult or impossible to obtain, in view of the complexity of the maps structures.

We note that a *minimum* orbital eccentricity is actually necessary for capture when the planetary mass is just below the critical value 1–5 $\times 10^{-5} M_\star$ (see the upper panels of Figs. 7 and 8). This is in agreement with the results of Weidenschilling and Jackson (1993), which can also be derived from Eq. (28): for a given value of the planetary mass, the condition $|\sin \theta_1| \leq 1$ requires that e_g be larger than a given value e_{min}. We have checked that the values of e_{min} derived by Weidenschilling and Jackson and from Eq. (28) agree within 10–20%, once the same stellar and planetary masses are used. As the planetary mass is increased, however, *all* the particles with initial

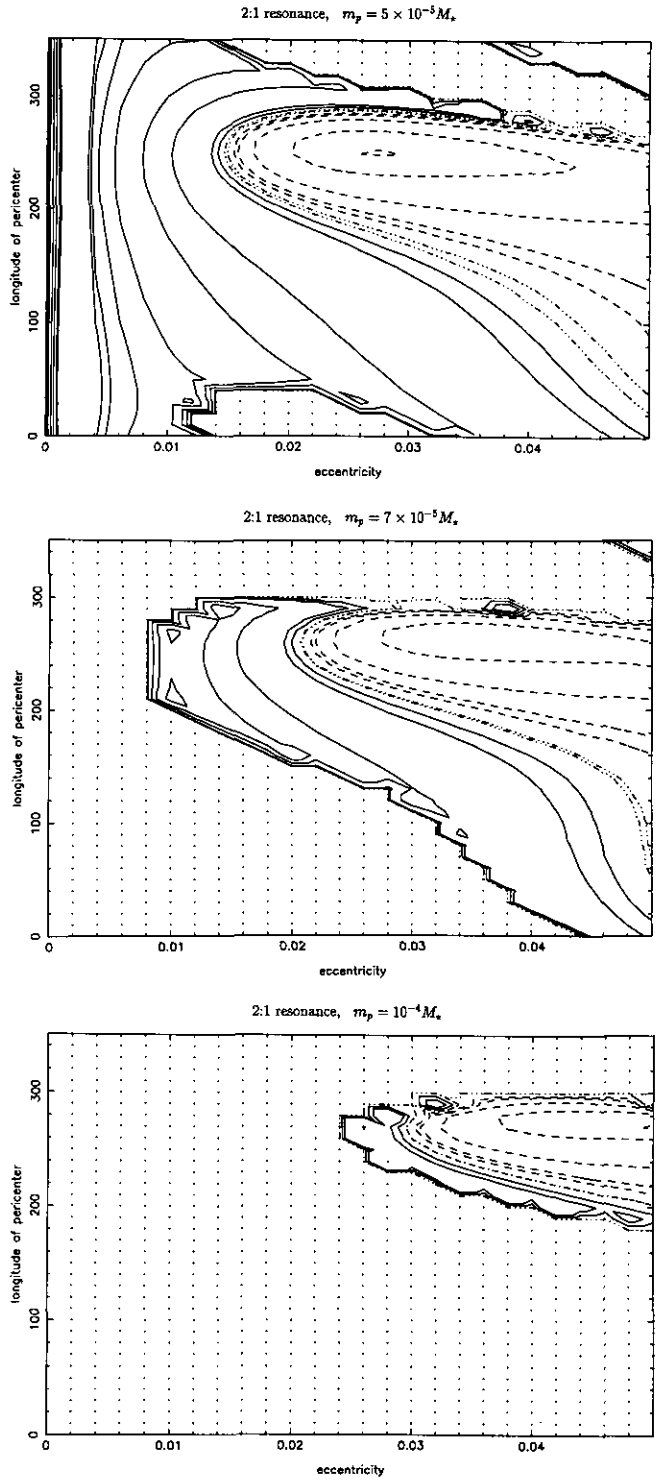

FIG. 7. Maps showing the regions of capture for the 1 : 2 resonance. The abscissa is the initial orbital eccentricity of the grain, and the ordinate is its initial longitude of periapse. The grain is released at 22.2 AU, and $\beta = 0.3$. The dotted regions correspond to capture into the resonance. In the rest of the map, the solid level curves link points corresponding to the same net *increase* of eccentricity. The dashed level curves show points corresponding to the same *decrease* of eccentricity. From top to bottom, the planetary masses are respectively 5×10^{-5} $M_\star$, 7×10^{-5} $M_\star$, and 10^{-4} $M_\star$, i.e., 25, 35, and 50 Earth masses, respectively.

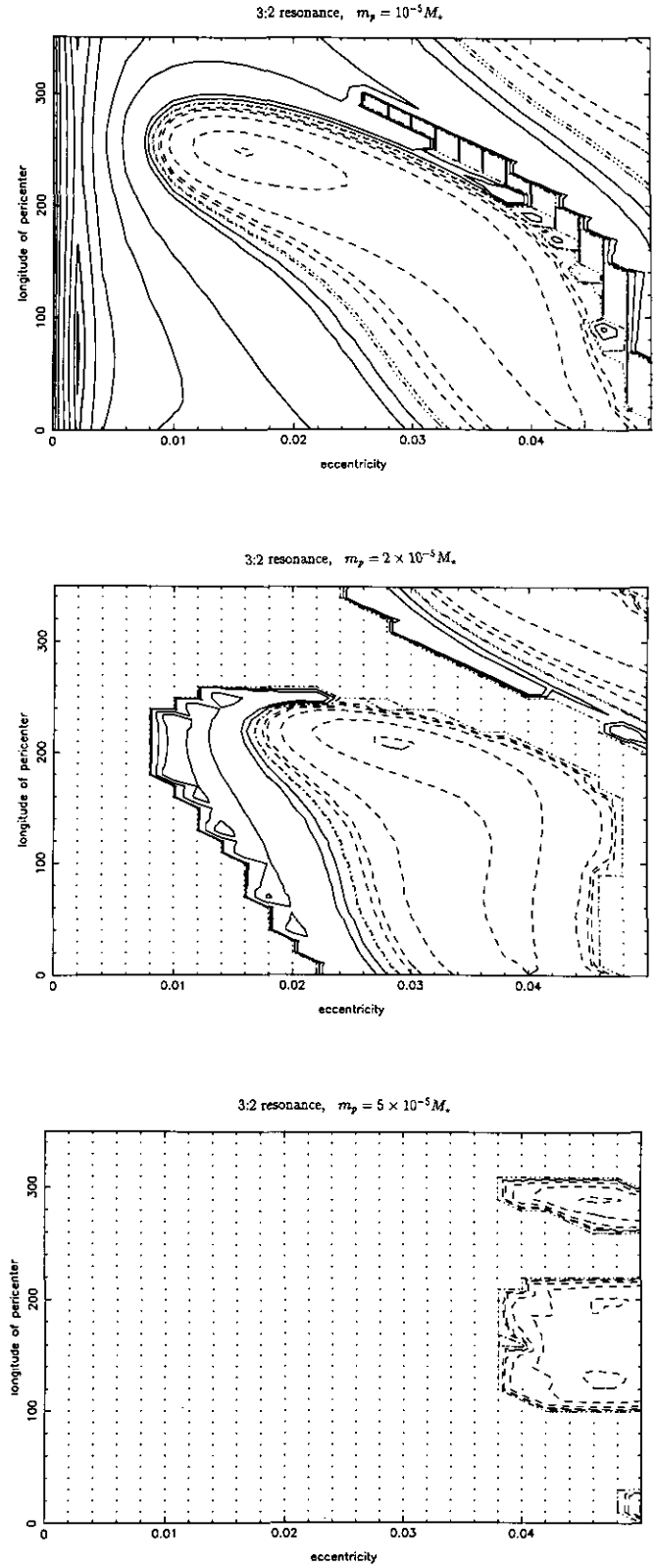

FIG. 8. The same as in Fig. 7 for the 2 : 3 resonance. From top to bottom, the planetary masses are respectively 10^{-5} $M_\star$, 2×10^{-5} $M_\star$, and 5×10^{-5} $M_\star$, i.e., 5, 10, and 25 Earth masses, respectively. For clarity, the dots (capture into the resonance) have been replaced by vertical lines in the upper panel.

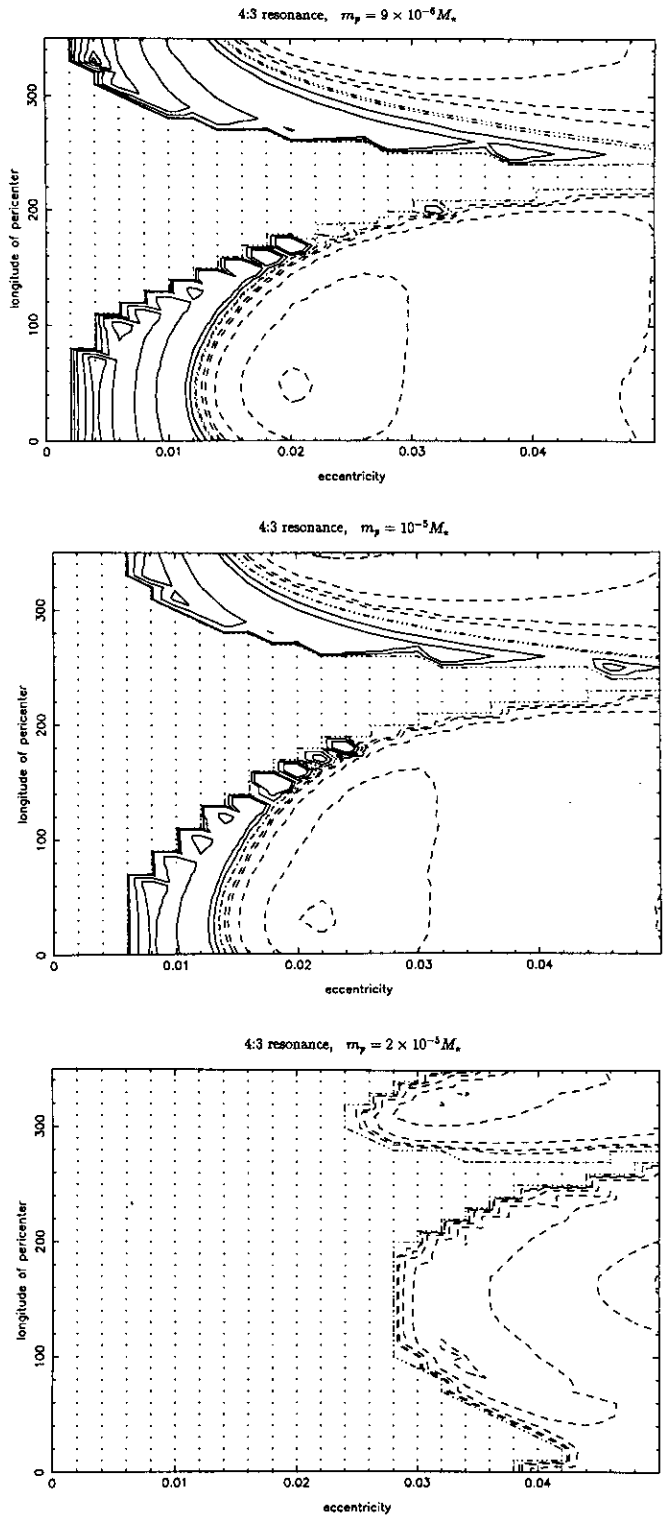

FIG. 9. Same as Fig. 7 for the 3 : 4 resonance. From top to bottom, the planetary masses are respectively $9 \times 10^{-6} M_\star$, $10^{-5} M_\star$, and $2 \times 10^{-5} M_\star$, i.e., 4.5, 5, and 10 Earth masses, respectively.

eccentricities *smaller* than a given value are captured (see the lower panels of Figs. 7, 8, and 9). This paradox stems from the fact that for a sufficiently massive planet (several times $10^{-5} M_\star \sim 5$ Earth masses), the eccentricity e_g in Eq. (28) cannot be considered as constant. For such massive planets, the resonance *itself* is able to pump up the eccentricity of the particles above e_{min}, so that a self-consistent approach must be used. This point is now examined in more details.

5.4. *Osculating Phase Space*

In order to clarify the importance of the phase θ_1 at the entrance into the resonance, we examine here two kinds of cases, one corresponding to noncapture, and one corresponding to capture. This point is illustrated in Fig. 10, where the evolution of $(e_g \cos(\theta_1), e_g \sin(\theta_1))$ is shown for two integrations, with various initial eccentricities and argument of pericenter for the grain. The planetary mass is $2 \times 10^{-5} M_\star$. The plots on the right are for an initial eccentricity of 0.007 and an initial longitude of the pericenter of 180°, while those on the left are for $e_g = 0.005$ and $\tilde{\omega}_g = 0°$.

The upper panels show the crossing, without capture, through the 1 : 2 resonance. The critical angle θ_1 first circulates in the clockwise direction. Due to the dissipation, the circulation orbit constantly shifts to the left while the grain approaches the resonance. At the entrance into the resonance, the eccentricity increases (upper left panel) or decreases (upper right panel), depending on the initial phase. The grain then crosses the resonance, while the critical angle starts a new circulation, now in the counterclockwise direction. The net increase (or decrease) of eccentricity can be understood by remembering that the eccentricity is pumped up by the resonance in the lower half of the plane, $\sin \theta_1 \leq 0$, and is damped in the upper half; see the discussion after Eqs. (27).

The plots in the lower panels show the capture into the 2 : 3 resonance. In this case, the critical angle begins in circulation and ends up librating near $\theta_1 = 180°$, with an average value of $\sin \theta_1$ which is negative. This is normal, since energy must be provided to the grain. The critical moment occurs when $\dot{\theta}_1$ changes its sign for the first time. We refer to the corresponding point as the "inversion point." Remember that all during the process, the instantaneous zones of libration surrounding L, i.e., the bean shaped curves shown in Fig. 2a, are constantly shifting toward the left due to the steady increase of C_1 (Eq. (19)). Note that the speed of this shift depends *only* on the dissipative term α and on geometrical factors. In particular, it is *independent* of the planet mass and of the phase θ_1.

If the inversion point occurs in the upper half of the plane, then the eccentricity is damped by the resonance at that point, while the bean-shaped libration curves go away to the left of the plane. Thus, the particle "falls" rapidly into the inner circulation zone and crosses the resonance. This case is illustrated in the upper right panel of Fig. 10.

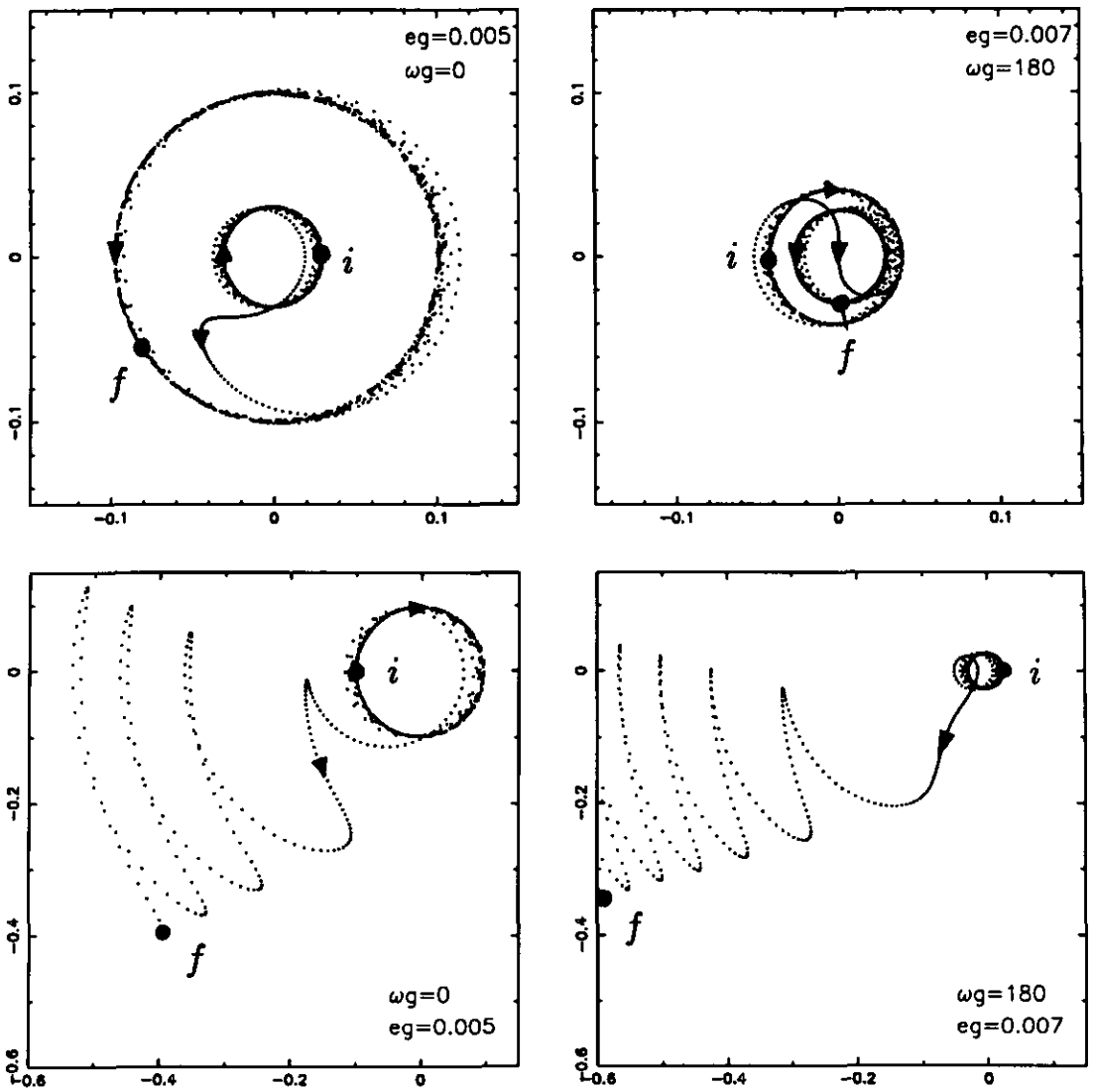

FIG. 10. The evolution of the resonance variables $e_g \sin(\theta_1)$, $e_g \cos(\theta_1)$ for two integrations with different values of the initial eccentricity (0.005 and 0.007) and the initial argument of pericenter (0° and 180°). The plots at the top show the crossing of the 1 : 2 resonance, and the plots at the bottom show the trapping into the 2 : 3 resonance. The points labelled i and f are the initial and final points, respectively. The arrows indicate the direction of evolution.

If the inversion point occurs in the lower half of the plane, then the eccentricity increases at that point due to the resonance. Again, the bean-shaped libration curves move to the left. Thus the capture into resonance depends upon the swiftness of the point in following up the evolution of the libration curves. In the example shown in Fig. 10 (upper left panel), the grain has no time to follow up this evolution. This point is detailed in Fig. 11.

In this figure, the "osculating phase space" is shown. Specifically, for each panel, several curves corresponding to the instantaneous value of C_1 of the particle are drawn, for various values of the quantity C_2. In other words, in a given diagram, the Mexican hat surface is fixed, and each curve corresponds to a different intersecting plane P (see Fig. 1a). In the present case, we see that the point representing the grain is not fast enough to go around the lower tip of one of the bean-shaped curves, so that it is enclosed in the inner circulating zone, while the libration curves move rapidly to the left. In Fig. 11, the inversion point occurs at the time labelled $T0 + 29\Delta T$, and the entrance into the inner circulation zone occurs between the times $T0 + 34\Delta T$ and $T0 + 38\Delta T$.

If the inversion point occurs closer to 180°, the libration zones are smaller, and the libration period is also smaller. This gives time for the point to catch up to the motion of the libration curves (lower panels of Fig. 10). Details on

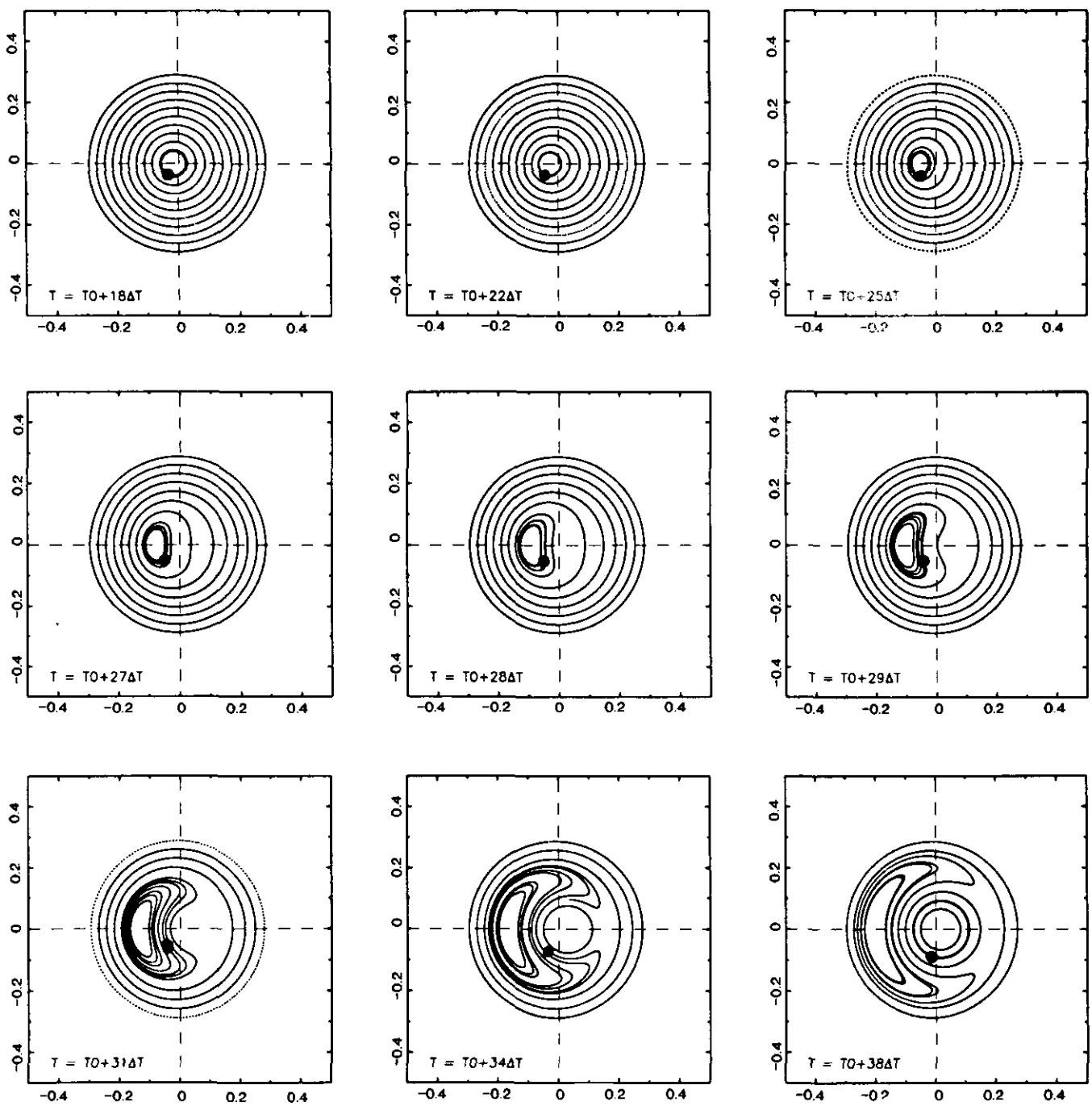

FIG. 11. Osculating phase space for some points shown in the upper left panel of Fig. 10. The interval ΔT corresponds to 256.3 years, i.e., four revolutions of the planet. The dot is the actual position of $e_g \sin(\theta_1)$, $e_g \cos(\theta_1)$. See the text for details.

the trajectory corresponding to the left panels of Fig. 10 are given in Fig. 12. For each position of the point, we calculate the osculating trajectory. The latter corresponds to the trajectory that would follow the point in the conservative case, with the instantaneous values of C_1 and C_2 of the particle. In the first case, we see how the particle is trapped into an inner circulation (Fig. 12a). In the second case, we see that the point has time to go around the lower tip of the libration curve; then it is "pushed" toward the left by the bean shaped curve, until the inversion point is reached again near 180°, and the process is resumed (Fig. 12b).

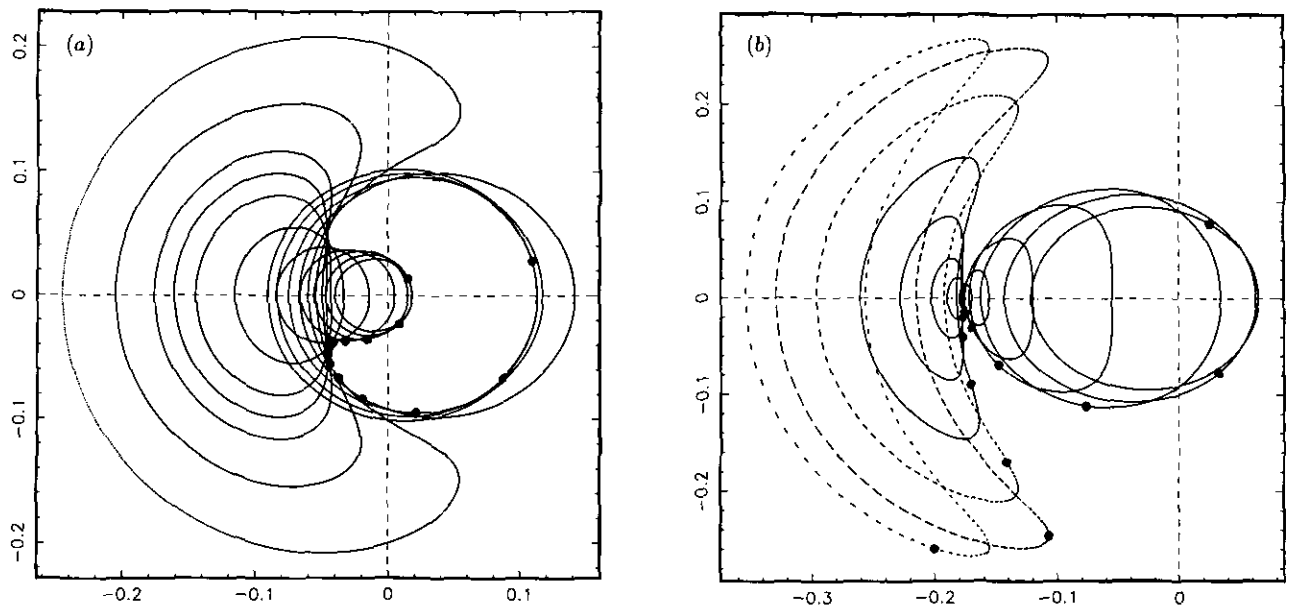

FIG. 12. (a) Osculating phase curves for each point shown in Fig. 11. Each of these solid curves would be the trajectory followed by the dot if the PR drag were suddenly removed. (b) The same in a case of capture, corresponding to the lower left panel of Fig. 10.

6. CONCLUSIONS

We have derived the averaged equations of motion of a circumstellar grain near a first order resonance with a planet, in the presence of PR drag. The integration of these equations has allowed us to answer a certain number of questions concerning the mechanism of capture into a resonance of a micrometer-sized grain orbiting a star such as β Pictoris.

We give a topological interpretation of the resonance effect, in which two surfaces steadily evolve in the phase space, under the effect of dissipation (Fig. 1). This yields the main features of the capture. In particular, we show why the capture must occur at an *outer* mean motion resonance only, and why the eccentricity should increase like $\sqrt{t}$, right after the capture, where t is the time.

The question of escape from the resonance at high eccentricity is still an open problem, since our equations are no longer valid for eccentricities larger than ~0.1, and since we use only averaged equations. However, we show that the trapping time in a given resonance is comparable to the decay time to the star due to PR drag alone. In that sense, the resonances can accumulate material just outside the planetary orbit.

The problem of capture probability is also a difficult one, because of the nonadiabaticity of the motion at the entrance into the resonance, at least with the parameters used in our models (micrometer-sized particles, planetary mass smaller than about one half of Saturn's mass). Only for jovian planets and/or particles larger than ~10 μm does the evolution of the grains in the phase space become adiabatic (Eq. (35)).

We show that the capture of a grain into a resonance critically depends on the orbital eccentricity and on the value of the critical argument of rersonance just at the entrance into the resonance. Maps of capture/noncapture regions vs these two parameters are derived numerically for the 1 : 2, 2 : 3, and 3 : 4 resonances (Figs. 7–9). They show the complexity of the capture regions, an indication that an analytical derivation of these regions is likely to be difficult. Interestingly enough, however, these diagrams show that a uranian or larger planet is able to trap most of the grains into the 1 : 2 resonance, while ~5 Earth masses are sufficient to trap grains into the 3 : 4 resonance, if the grains have initial eccentricities smaller than a few percent.

Consequently, reasonably small planetary objects orbiting a star may have important dynamical effects on the circumstellar dust disk. As shown in Paper 1, future observations at higher angular resolution could provide important constraints on the presence of planets through the observation of the associated disk.

APPENDIX A. LIST OF SYMBOLS

a_g, a_p Orbital semimajor axis of the grain, of the planet.
A A combination of various coefficients; see the definitions following Eqs. (14).
A^q_{pg} Combination of Laplace coefficients; see Eqs. (11).
B A combination of various coefficients; see the definitions following Eqs. (14).

b_s^q Laplace coefficient.
B_{pg}^q Combination of Laplace coefficients; see Eqs. (11).
c Velocity of light.
C A combination of various coefficients; see the definitions following Eqs. (14).
C_1, C_2 Integrals of motion near a Lindblad resonance; see Eqs. (18).
D' A combination of various coefficients; see Eqs. (17) and following.
D_{pg}^q Combination of Laplace coefficients; see Eqs. (11).
e_{eq} Equilibrium eccentricity reached under the combined effects of resonance and Poynting–Robertson drag; see Eq. (28).
e_g, e_p Orbital eccentricity of the grain, of the planet.
e_{lib} Eccentricity corresponding to the stable libration point L; see Fig. 2.
f Factor of order unity depending weakly on q; see Eq. (12).
F Total Hamiltonian acting on the grain.
f_p Precession rate of the planet orbit pericenter.
$\mathbf{F}_{grav}$ Gravitational force due to the star.
$\mathbf{F}_{PR}$ Poynting–Robertson drag force.
$\mathbf{F}_{rad}$ Total radiation force.
G Delaunay variable associated with angular momentum.
$\mathcal{G}$ Gravitational constant.
H $\sqrt{2J_1}\sin\theta_1$, one component of the eccentricity vector (see Eq. (13)).
J_1, J_2, J_3 Conjugate moments of the angles θ_1, θ_2, θ_3.
K $\sqrt{2J_1}\cos\theta_1$, one component of the eccentricity vector (see Eq. (13)).
L Delaunay variable associated to energy.
$L_\star$ Luminosity of the star.
$L_\odot$ Luminosity of the Sun.
m_g, m_p Mass of the grain, of the planet.
$M_\star$, $M_\odot$ Mass of the star, of the Sun.
M_{pg}^q Combination of Laplace coefficients; see Eqs. (11).
n_g, n_p Mean motion of the grain, of the planet.
P Intersecting plane; see Fig. 1.
q Integer defining a $(q+1):q$ mean motion resonance ($(q+1)n_p = qn_g$).
Q Radiation pressure efficiency.
R Perturbing function due to the planet.
$\mathbf{r}$ Position vector from the star to the current point.
$\mathbf{r}_g$, $\mathbf{r}_p$ Position vector from the star to the grain, to the planet.
r_{gp} Distance from the grain to the planet.
R_a, R_H, R_K Combinations of various coefficients; see the definitions following Eqs. (14).
s Radius of the grain.
S Energy flux at the grain.
S_1 A combination of various coefficients; see the definitions following Eqs. (14).
sw Ratio of stellar wind drag to Poynting–Robertson drag.
T_{evol} Time scale for evolution of the resonance phase space; see Eq. (24).
T_{lib} Libration period near the stable libration point L; see Eq. (25).
T_{orb} Orbital period of the grain.
U Negative of potential energy.
$\mathbf{u}_r$ Unit vector in the direction of incident radiation.
$\mathbf{v}$ Velocity of the grain.
w_{lib} Width of the libration zone; see Fig. 2.
X_j Components of the Poynting–Robertson drag ($j = 1, 2$ in the planar case).
Z Third dimension in the $OHKZ$ space; see Fig. 1.
Z_{min} Minimum ordinate on the Mexican hat surface; see Fig. 1.
α Dissipation coefficient parameterizing the Polynting–Robertson drag (Eq. (4)).
β Ratio F_{rad}/F_{grav} of the radiation to the gravitational forces (Eq. (2)).
γ A combination of various coefficients; see the definitions following Eqs. (14).
δ^q Kronecker symbol: 1 if $q = -2$, 0 otherwise.
Δn $(q+1)n_p - qn_g$, the distance to exact resonance.
ε The ratio $m_p/M_\star$ of the planetary mass to the stellar mass.
ζ_j Components of the grain velocity ($j = 1, 2$ in the planar case).
η_j Cartesian coordinates of the grain ($j = 1, 2$, in the planar case).
θ_1 Critical argument of the Lindblad resonance, $(q+1)\lambda_p - q\lambda_g - \tilde{\omega}_g$.
θ_2 Critical argument of the corotation resonance, $(q+1)\lambda_p - q\lambda_g - \tilde{\omega}_p$.
θ_3 $\lambda_g - \lambda_p$.
λ_g, λ_p Mean longitude of the grain, of the planet.
Λ Conjugate moment of the time.
μ $\mathcal{G}(m_g + M_\star)$.
ξ Ratio a_p/a_g of the planetary orbital semimajor axis to the grain's orbital semimajor axis.
ρ $\sqrt{1-e_g^2}$.
σ Geometrical cross-section of the grain.
$\tilde{\omega}_g$, $\tilde{\omega}_p$ Longitude of pericenter of the grain's orbit, of the planetary orbit.

ACKNOWLEDGMENTS

We thank A. A. Jackson and S. J. Weidenschilling for several discussions and also S.J.W. for a careful review of this paper. An anonymous referee made several constructive comments. D. Lazzaro was partly supported by the Brazilian National Research Council, Proc. CNPQ 201053/90.0. Finally, D. Lazzaro, F. Roques, and B. Sicardy were partly supported by the French Programme National de Planétologie.

REFERENCES

ARTYMOWICZ, P., C. BURROWS, AND F. PARESCE 1989. The structure of the Beta Pictoris circumstellar disk from combined IRAS and coronographic observations. *Astrophys. J.* **337,** 494–513.

BEAUGÉ, C., AND S. FERRAZ-MELLO 1993. Resonance trapping in the primordial solar nebula: The case of a Stokes drag dissipation. *Icarus* **103,** 301–318.

BORDERIES, N., P. GOLDREICH, AND S. TREMAINE 1984. Unsolved problems in planetary ring dynamics. In *Planetary Rings* (R. Greenberg and A. Brahic, Eds.), pp. 713–734. Univ. of Arizona Press, Tucson.

BROUWER, D., AND G. HORI 1961. Theoretical evaluation of atmospheric drag effects in the motion of an artificial satellite. *Astron. J.* **66,** 193–210.

BULIRSCH, R., AND J. STOER 1966. Numerical treatment of ordinary differential equations. *Numer. Math.* **8,** 1–13.

BURNS, J. A., P. L. LAMY, AND S. SOTER 1979. Radiation forces on small particles in the Solar System. *Icarus* **40,** 1–48.

DERMOTT, S. F., R. F. GOMES, D. D. DURDA, B. Å. S. GUSTAFSON, S. JAYARAMAN, Y. L. XU, AND P. D. NICHOLSON 1992. Dynamics of the Zodiacal cloud. In *Chaos, Resonance and Collective Dynamical Phenomena in the Solar System* (S. Ferraz-Mello, Ed.), IAU Symposium No. 152, pp. 333–347. Kluwer Academic, Norwell, MA.

DERMOTT, S. F., S. JARAYAMAN, Y. L. XU, AND J. C. LIOU 1993a. IRAS observations show that the Earth is embedded in a Solar ring

of asteroidal dust particles in resonant lock with the planet. *Bull. Am. Astron. Soc.* **25,** 1116.

DERMOTT, S. F., S. JARAYAMAN, Y. L. XU, AND J. C. LIOU 1993b. IRAS observations of a ring around the Sun: Asteroidal particles in resonant lock with the Earth. Preprint.

FERRAZ-MELLO, S. 1985. Resonance in regular variables. I. Morphogenetic analysis of the orbits in the case of a first-order resonance. *Celest. Mech.* **35,** 209–220.

FERRAZ-MELLO, S. 1987. Expansion of the disturbing force-function for the study of high-eccentricity librations. *Astron. Astrophys.* **183,** 397–402.

FERRAZ-MELLO, S. 1992. Averaging the elliptic asteroidal problem with a Stokes drag. In *Physics and Dynamics of the Small Bodies of the Solar System* (D. Benest and Cl. Froeschlé, Eds.), pp. 45–60, Ed. Frontières, Gif-sur-Yvette.

GOLDREICH, P., AND S. TREMAINE 1982. The dynamics of planetary rings. *Ann. Rev. Astron. Astrophys.* **20,** 249–283.

GOLDREICH, P., S. TREMAINE, AND N. BORDERIES 1986. Towards a theory of Neptune arc rings. *Astron. J.* **92,** 490–494.

GONCZI, R., CH. FROESCHLÉ, AND C. FROESCHLÉ 1982. Poynting–Robertson drag and orbital resonance. *Icarus* **51,** 633–654.

GREENBERG, R. 1978. Orbital resonance in a dissipative medium. *Icarus* **33,** 62–73.

JACKSON, A. A., AND H. A. ZOOK 1989. A solar system dust ring with the Earth as its shepherd. *Nature* **337,** 629–631.

JACKSON, A. A., AND H. A. ZOOK 1992. Orbital evolution of dust particles from comets and asteroids. *Icarus* **97,** 70–84.

KARY, D. M., J. J. LISSAUER, AND Y. GREENZWEIG, 1993. Nebular gas drag and planetary accretion. *Icarus* **106,** 288–307.

LISSAUER, J. J. 1985. Shepherding model for Neptune's arc ring. *Nature* **318,** 544–545.

MALHOTRA, R. 1993. Orbital resonances in the Solar System: Strengths and weaknesses. *Icarus* **106,** 264–273.

MEYER-VERNET, N., AND B. SICARDY 1987. On the physics of resonant disk–satellite interaction. *Icarus* **69,** 157–175.

PATTERSON, C. W. 1987. Resonance capture and the evolution of the planets. *Icarus* **70,** 319–333.

PEALE, S. J. 1976. Orbital resonances in the solar system. *Ann. Rev. Astron. Astrophys.* **14,** 215–245.

PEALE, S. J. 1986. Orbital resonances, unusual configurations, and exotic rotation states among planetary satellites. In *Satellites* (J. A. Burns and M. S. Matthews, Eds.), pp. 159–223. Univ. of Arizona Press, Tucson.

ROQUES, F., H. SCHOLL, B. SICARDY, AND B. SMITH 1994. Is there a planet around β-Pictoris? Perturbation of a planet on a circumstellar dust disk. 1. Numerical model. *Icarus* **108,** 37–58.

SCHOLL, H., F. ROQUES, AND B. SICARDY, 1993. Resonance trapping of circumstellar dust particles by an alleged planet. *Celest. Mech.* **56,** 381–393.

SICARDY, B. 1991. Numerical exploration of planetary arc dynamics. *Icarus* **89,** 197–219.

SICARDY, B., C. BEAUGÉ, S. FERRAZ-MELLO, D. LAZZARO, AND F. ROQUES 1993. Capture of grains into resonances through Poynting–Robertson drag. *Celest. Mech.* **57,** 373–390.

SMITH, B., AND R. J. TERRILE 1984. Circumstellar disk around β Pictoris. *Science* **226,** 1421–1424.

WEIDENSCHILLING, S. J. 1977. Aerodynamics of solid bodies in the solar nebula. *Mon. Not. R. Astron. Soc.* **180,** 57–70.

WEIDENSCHILLING, S. J., AND D. R. DAVIS 1985. Orbital resonances in the solar nebula: Implications for planetary accretion. *Icarus* **62,** 16–29.

WEIDENSCHILLING, S. J., AND A. A. JACKSON 1993. Orbital resonances and Poynting–Robertson drag. *Icarus* **104,** 244–254.